THE EFFECTS OF CO-60 GAMMA RADIATION ON THE THERMAL DECOMPOSITION OF CARBONATE COMPOUNDS

by

DANNY WILLIAM LABELLE

B. S., North Carolina State University, 1966

A MASTER'S THESIS

submitted in partial fulfillment of the

requirements for the degree

MASTER OF SCIENCE

Department of Nuclear Engineering

KANSAS STATE UNIVERSITY

Manhattan, Kansas

1969

Approved by:

Major Professor

TABLE OF CONTENTS

LIST OF TABLES

LIST OF FIGURES

LIST OF FIGURES (continued)

LIST OF FIGURES (continued)

NOMENCLATURE

h_c	Convective heat transfer coefficient from gas to thermocouple, cal/sec·cm^2·deg
h_r	Radiative heat transfer coefficient from thermocouple to confining walls, cal/sec·cm^2·deg
k	Reaction rate constant, seconds^{-1}
T_g	Temperature of gas, degrees Centigrade
T_t	Temperature measured by thermocouple, degrees Centigrade
T_w	Temperature of confining walls, degrees Centigrade
t	Time from start of thermal decomposition, seconds
W_l	Weight lost during thermal decomposition, grams
W_s	Weight of dried solid, grams
w	Weight of solid after time t, grams
w_o	Initial weight of solid, grams
α	Fractional decomposition of solid ($\alpha = 1 - \frac{w}{w_o}$), dimensionless

1.0 INTRODUCTION

Carbonate compounds are constituents and impurities of concrete, a common material in nuclear reactor shielding. The evolution of carbon dioxide gas from the decomposition of these compounds to an oxide form in a high radiation-temperature environment over prolonged periods of time could cause degradation of concrete shielding, and thus represents a potential hazard in high power nuclear reactor operation. An absence of data on this type of reaction has led to this investigation which, although not conclusive, should serve as a useful reference for future work.

The purpose of this research is to study the non-equilibrium reaction kinetics of the thermal decomposition of irradiated and non-irradiated zinc and manganese carbonate salts in an inert atmosphere of helium by measuring the carbon dioxide released. These two salts have been chosen because their low temperature decomposition makes the study of these materials compatible with the temperature limitations of the equipment used. Co-60 gamma radiation was used during this study but further work with reactor radiations is encouraged.

The kinetics of thermal decomposition of crystalline compounds, i.e.,

$$A(\text{solid}) \rightarrow B(\text{solid}) + C(\text{gas})$$

is commonly studied for cases where B is insoluble in A. Effects of various types of nuclear radiation on the kinetics of this type of decomposition have been studied for nitrate compounds, (1,2,3,4) permanganates, (5,6) sodium bromate, (7) α-lead azide, (8) silver (9) and lead (10) oxalates. Research of this nature, however, has been hampered by the inability of investigators to give completely self-consistent accounts of the kinetics

of decomposition. Particular problems include the complexities involved in showing whether the compound passes directly to the reaction products or through one or more intermediate states, and the difficulty in obtaining positive evidence to support a particular mechanism for the reaction. These and other problems have led to a general lack of interest in research on radiation effects on thermal decomposition.

Equilibrium and non-equilibrium reaction kinetics for the thermal decomposition of non-irradiated carbonates have been investigated using thermogravimetric analysis (11,12,13,14,15) and measurement of carbon dioxide pressure (16,17,18). These methods could also be applied to the study of irradiated carbonate decomposition as has been done in the latter study by Mohanty and Ray (16). Another and apparently simpler method, however, gas chromatography, was used in this research as an analytical means for studying the reaction kinetics. The speed of analysis and its high sensitivity makes gas chromatography an excellent method for quantitatively analyzing the carbon dioxide released in the reaction.

2.0 THEORY AND REVIEW OF LITERATURE

2.1 Kinetics of Thermal Decomposition of Solids

2.1.1 General Form of the Decomposition Curve and Descriptive Terminology

For solids which decompose during isothermal heating according to the following reaction

$$A(\text{solid}) \rightarrow B(\text{solid}) + C(\text{gas}) \qquad (1)$$

the experimental results are most commonly presented as the fractional decomposition (α) or equivalent parameters ($\frac{d\alpha}{dt}$, etc.) as a function of time t for a series of constant temperatures (isotherms). Whenever possible, these data are supported by direct observations of the form and distribution of the solid reaction product.

In the general case, the decomposition curve for the reaction has the features illustrated in Fig. 1, although any of these features, except the maximum rate, may be absent in specific cases. The features as explained by Young (19) include an initial rapid evolution of gas A. The form of the curve in this region is usually first order, i.e., reaction depends only on the decomposition of one component.

This initial process is then followed by section B, termed the induction period, and characterized by a slow evolution of gas. In some cases, the reaction is scarcely measurable in this region and some means of arbitrarily defining the induction period has to by employed.

When a true induction period occurs, it is invariably succeeded by the acceleratory period, designated by C, which normally extends up to fractional decompositions between 0.1 and 0.5, although values above this range are

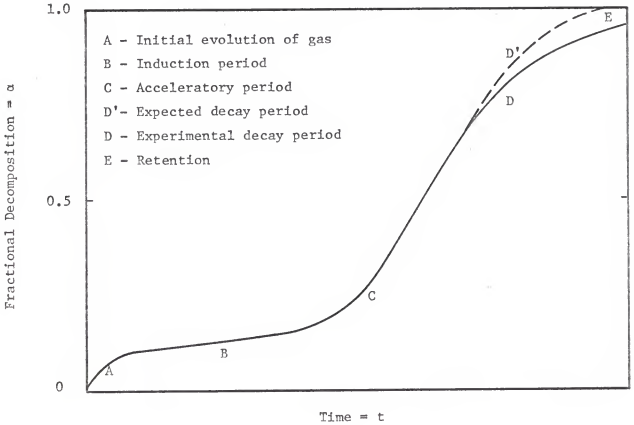

Fig. 1. The generalized isothermal decomposition curve.

possible. The acceleratory period is the part of the deomposition curve which is studied the most intensively. It is customary to fit expressions of the form

$$\alpha = f(\exp kt) \tag{2}$$

or

$$\alpha = f(kt^n) \tag{3}$$

to the acceleratory period and nearly perfect fits have been obtained with these simple expressions, but normally it is necessary to compromise and to introduce an adjustable time parameter, t_o, such that

$$\alpha = f(t-t_o)^n \ . \tag{4}$$

The decay period D is both more difficult to analyze satisfactorily and less valuable for interpretation because it depends on the details of the particle size distribution at this stage of the decomposition. In cases where particle size effects can be eliminated, however, the decay period can normally be analyzed according to a power function representing a contracting envelope of some kind or a first-order expression.

Between sections C and D lies the transition region. This region defines the maximum rate of the decomposition as evidenced by an inflection point.

The final region of the decomposition curve, labeled E, results from the lack of reproducibility of the decay period at high degrees of decomposition. The deviation of the experimental decay curve D from the expected value D', obtained by assuming the analytical function applicable throughout the major portion of D is valid up to $\alpha = 1$, is called the retention. This nonreproducible phenomenon is believed to arise from a combination of parti-

cle size effects, the reduction of chemical reactivity by poisoning or sintering, or the chemisorption of product gas on the solid product.

2.1.2 The Topochemical Nature of Solid Decompositions

The analysis of decomposition curves, the acceleratory period in particular, has always been based on geometrical principles. This approach can be attributed to the work of Langmuir (20) on the dissociation of $CaCO_3$ into CaO. In applying the phase rule to this reaction, Langmuir concluded that in order for $CaCO_3$ to form a new phase CaO instead of a solid solution, the reaction must occur at the boundary between the phases.

In subsequent studies on decomposition, Hinshelwood and Bowen (21) found that the activation energy was dependent on the extent of the reaction interface which was not necessarily the external surface of a crystal. They further showed that light crushing of partly decomposed ammonium dichromate exposed fracture planes covered with reaction products, whereas on further grinding the interior regions of the particles were observed to have not decomposed. Also the initial reaction rate on grinding was found to be larger than could be explained by the increase in the surface area, indicating the creation of internal surfaces.

The present concept of reaction nuclei was introduced by MacDonald and Hinshelwood (22). Working with silver oxalate, they presented indirect evidence for the formation and growth of autocatalytically active nuclei. They suggested that autocatalysis could account for the acceleration in the thermal decomposition of silver oxalate either through increases in the surface area of the solid or through the presence of nuclei of the product silver. Since this acceleration was not eliminated on further grinding of the oxalate, they concluded that nuclei formation and growth were occurring. They also showed

that nucleation occurred on the external surface. Kinetic support for their findings was later provided by Roginskii and Shultz (23) in studies of the decomposition of potassium permanganate. Further evidence of the existence of nuclei was provided by the works of Kohlschütter (24) and Garner and his co-workers (25,26,27). It has been the work of these researchers which has led to the general acceptance that a topochemical model, nucleus formation and growth by an interfacial mechanism, accounts for the kinetics of the acceleratory period.

2.1.3 The Theory of Solid Decompositions

The topochemical model showed that the decomposition of solids was initiated by the formation and growth of nuclei. These nuclei, sometimes called germ nuclei, are composed of highly disorganized material and are formed on the external surfaces of the solid or at surface cracks, dislocations, and lattice imperfections either by highly localized decomposition which has occurred at low temperatures before decomposition proper, or by decomposition suffered during rapid heating to the proposed decomposition temperature. Nucleation is favored at these sites because the disorganized surface has fewer bonds to be broken than a well-coordinated normal surface.

The reaction then spreads from these nuclei both along the surface and into the interior of the solid with decomposition occurring all along the reaction interface. That this reaction interface then advances at a constant rate has been confirmed in the majority of cases. Deviations from this ideal behavior do occur, however, since nucleation and growth can be influenced by impedance to the escape of gaseous products and by the size of the nuclei. Topley and Smith (28), for instance, found an impedance to the release of a

gaseous reaction product by layers of solid product while Cooper and Garner (27) have shown that small nuclei grow more rapidly than large ones.

Several attempts have been made to formulate general kinetic equations which mathematically conform with the topochemical model (29,30,31,32,33); such approaches consisted of making postulates of the laws of nucleus formation and growth. Common postulates are that the decomposition of the solid is unimolecular and that the reaction interface advances at a constant rate. Some earlier models were also based on homogeneous nucleation and the spherical growth of nuclei. These postulates led to kinetic equations which were deficient in that nucleus formation was found to be independent of the extent of the reaction or it was proportional to the volume of the undecomposed fraction of the material. This approach was later refined to include heterogeneous nucleation, which was noted in practice, and to allow for overlap or ingestion of germ nuclei by large nuclei.

One of the more detailed treatments of solids in the form of microcrystals is that of Mampel (34). His theory included the assumptions used by earlier investigators that the rate of formation of nuclei follows a unimolecular law and that the interface advances at a constant linear velocity. Then with the additional assumption that the microcrystals were isotropic spheres of uniform radius, Mampel derived a general expression for the rate of decomposition. Since this expression included the particle radius, it was useful in estimating the probable effects of particle size. In essence, Mampel divided each spherical particle into concentric shells. He then used probability considerations to incorporate the problems of overlapping and ingestion of the germ nuclei. An expression for the fractional decomposition as a function of time was then obtained by integrating over the shells. Since the expression was of an integral type, rigorous solutions were only

possible through numerical computer integration techniques. It was therefore necessary to make certain simplifying assumptions to arrive at more workable forms of the expression.

Three limiting cases are of interest. For the early part of the reaction where values of time are small, the fractional decomposition, α, was related by Mampel (34) to the time, t, by the equation

$$\alpha = at^4 . \tag{5}$$

For large particle radius, r, the intermediate decay region conformed to the equation

$$\frac{k_o t}{r} = 1 - (1-\alpha)^{1/3} \tag{6}$$

which is the one-third power law for a contracting sphere (35) with a constant velocity of propagation, k_o. Finally for small particle radius, the decomposition according to Mampel was governed by the equation

$$\ln(1-\alpha) = a - kt . \tag{7}$$

2.1.4 The Thermal Decomposition of Manganous Carbonate - $MnCO_3$

Razouk and co-workers (14) have carried out a limited study on the kinetics of the thermal decomposition of manganous carbonate. Their work was the only comprehensive analysis on non-equilibrium kinetics of this carbonate to be found in the literature up to the time of this work.

Using thermogravimetric analysis and continuous pumping off of the carbon dioxide released from the system, Razouk obtained fractional decomposition curves over a wide temperature range for both precipitated manganous

carbonate (Fig. 2) and crushed crystals of rhodochrosite (Fig. 3), the mineral form of the carbonate. Both sets of curves showed a decay period covering 80-90% of complete reaction. The decay period of the precipitated carbonate with an initial weight, w_o, and a weight, w, after time t was represented by

$$(w/w_o)^{1/3} = -kt + b \quad . \tag{8}$$

For the fractional decomposition defined as

$$\alpha = 1 - \frac{w}{w_o} \tag{9}$$

equation (8) can be rearranged to a form

$$1 - (1-\alpha)^{1/3} = kt + c \quad . \tag{10}$$

The decay period for rhodochrosite was likewise given by

$$\ln(1-\alpha) = -k't' \tag{11}$$

where k' is the reaction rate constant and $t' = t-t_o$, t_o being an induction period. Linear plots from work of Razouk (14) of $(w/w_o)^{1/3}$ and $\log_{10}(1-\alpha)$ against time (Figs. 4 and 5) gave direct verification of these expressions.

Comparison of these expressions with Mampel's theory show the decomposition of the precipitated carbonate followed the one-third power law of contracting spheres. The rhodochrosite deviated from this law, however, since it decomposed rapidly during the early stages and more slowly at the latter stages of the reaction. Razouk attributed this difference to the inhibited growth of nuclei in the rhodochrosite in view of the severe conditions of temperature and pressure under which its structure was formed. Possible inhibiting effects included the restriction of gas diffusion by the oxide layers formed and the possibility of oxide and carbon dioxide recombination at the

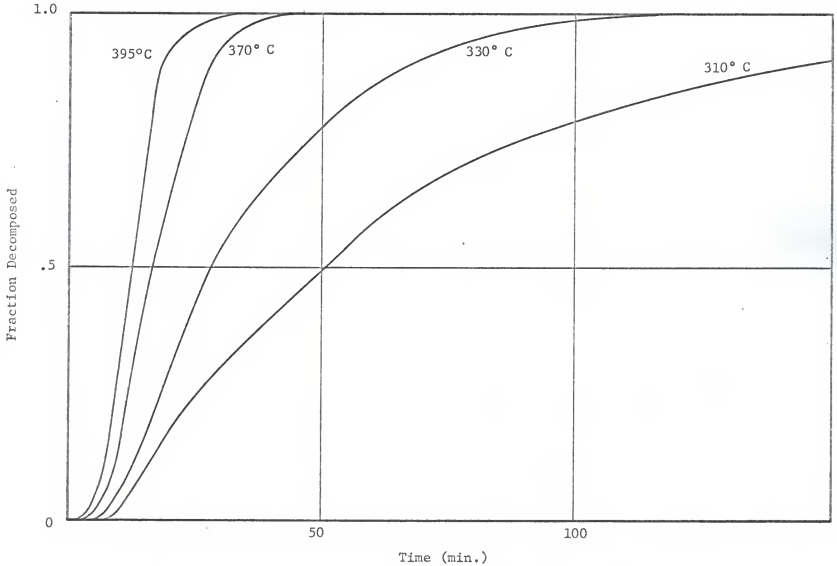

Fig. 2. Thermal decomposition curves of precipitated manganous carbonate at different temperatures as presented in the work of Razouk, et. al. (14).

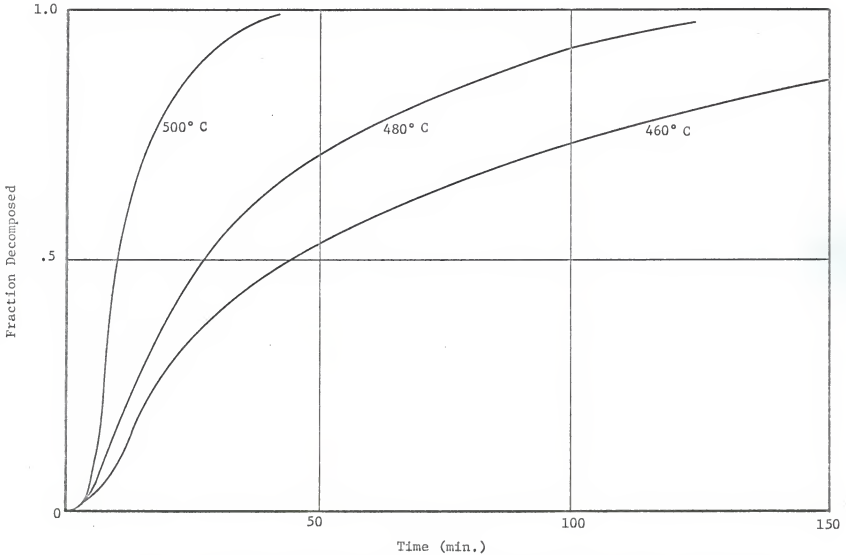

Fig. 3. Thermal decomposition curves of rhodochrosite at different temperatures as presented in the work of Razouk, et. al. (14).

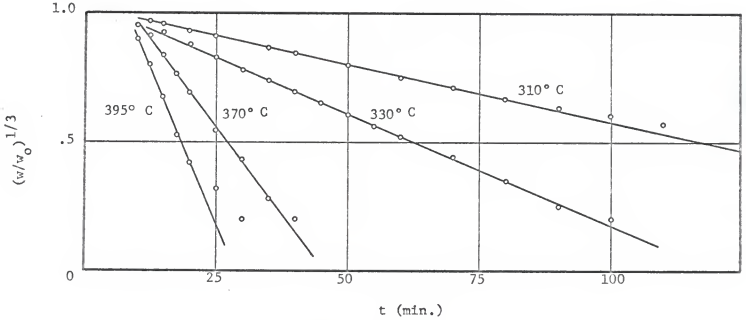

Fig. 4. Plot of $(\frac{w}{w_o})^{1/3}$ against time t, for thermal decomposition of precipitated manganous carbonate as presented in the work of Razouk, et. al. (14).

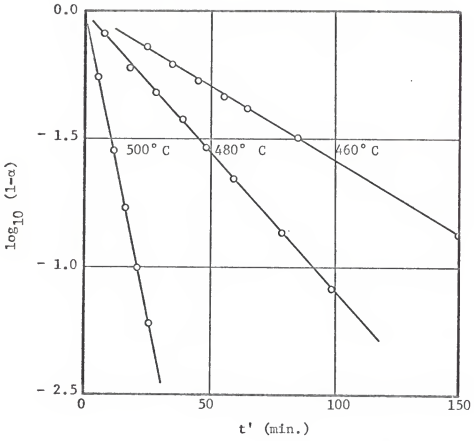

Fig. 5. Plot of $\log_{10}$ (1-α) against time t', for the decomposition of rhodochrosite as presented in the work of Razouk, et. al. (14).

interface. Also the restricted escape of the gas in any region of the reaction could catalytically assist the mechanism of nuclei growth.

In conclusion, the work of Razouk on manganous carbonate supported the view that the decomposition kinetics are dependent on the topography, structure and texture of the reactant matrix.

2.2 Gamma Radiation Damage in Crystalline Solids

2.2.1 The Interaction between Gamma Radiation and Crystalline Solids

The effects of various radiations on crystalline solids can be classified as primary or secondary. The primary effects are ionization (the displacement of electrons), the displacement of atoms from lattice sites, excitation of atoms and electrons without displacement, and transmutation of nuclei. The secondary effects would then consist of further excitation and disruption of the lattice structure by electrons or displaced atoms. Under this method of classification, gamma radiation, which carries no electric charge and has no rest mass, would be expected to produce primarily extensive ionization and electronic excitation, and secondarily atomic displacements.

The more important interaction mechanisms leading to these effects are the photoelectric effect, Compton scattering, and pair production. Through these interactions a quantum of gamma radiation may deposit some or all of its energy in its passage through the solid. For gamma radiation from common nuclear sources, the Compton effect has the largest cross section, except for targets of very high atomic number.

Damage to a crystalline solid from gamma collisions commonly results from atomic displacements which are produced by ejected electrons, recoil atoms, and the Seitz and Varley mechanisms (36,37). Damage can also result from the

liberation of heat when atoms do not receive enough energy for displacement but undergo strong vibratory motion at their lattice sites.

A nucleus or electron to which energy has been transferred by a collision is designated as a primary. High energy primaries interact with the electrons of a crystalline solid causing excitation and ionization. When their energies pass below the ionization threshold, elastic collisions with other atoms are predominant. From these collisions, damaging displaced atoms and vibratory heat are generated. This damage is manifested in the creation of point and line defects, and the breakage of chemical bonds in crystalline solids.

For gamma radiation of energy 1 MeV or less, the number of displaced atoms cm^{-3} sec^{-1} by the Compton electrons has been shown by Dienes and Vineyard (38) to be at a maximum in the very light elements and to decline rapidly with increasing atomic number, becoming zero for 1 MeV gammas and a displacement threshold of 25 eV, at atomic weight 125. For higher energy (in excess of 1 MeV) gamma radiation, the displaced atoms cm^{-3} sec^{-1} reach a maximum with intermediate or heavy elements.

2.2.2 The Effects of Gamma Radiation on the Decomposition of Crystalline Solids

That gamma radiation can induce decomposition of crystalline solids is expected since it does have a damage producing capability in these materials. The extensive work on the gamma radiation induced decomposition of nitrate compounds (1,2,3,4) has confirmed the existence of this effect.

Furthermore, the observation that the reaction products which resulted from these decompositions were similar to those released from the thermal decomposition of the nitrates have led to the speculation of possible mecha-

nisms for the reaction, none of which have been supported by conclusive evidence. Their applicability in the decomposition of other inorganic compounds is also questionable. Hennig (1) and Johnson (2) have agreed, however, that the breaking of weak atomic bonding in nitrates through ionization and excitation takes precedence over atomic displacement. Johnson has also suggested that electronic excitation energy when transferred to lattice vibrational energy could cause, in effect, high local temperatures which would be sufficient to break neighboring covalent and ionic bonds and thus account for the thermal nature of the decompositions of nitrates and perhaps other inorganic compounds.

Gamma radiation has also been observed to enhance the rate of thermal decomposition of crystalline solids (5,6,7,8,9,10,16). The best approach toward explaining this phenomenon is presented in the studies of Jach (39) on thermal decomposition at defects in α-lead azide, nickel oxalate, and sodium bromate. Using a combination of the theories of radiation damage and the topochemical model, he concluded that gamma irradiations prior to thermal decomposition of a crystalline solid increased the number of germ nuclei by the creation of lattice defects and led to subsequent regions of disorder in the material. The larger number of germ nuclei available to form growth nuclei then accounted for the increased decomposition rates.

3.0 DESCRIPTION OF EXPERIMENTAL APPARATUS

The basic equipment used in this research was a gamma irradiator, a high temperature furnace, and a gas chromatography system.

The gamma irradiator: The Kansas State University "Gammacell"-220 was used for the gamma irradiations of manganous and zinc carbonate. This unit, designed by Atomic Energy of Canada, Ltd., contained at delivery (March, 1965) approximately 4000 curies of cobalt-60. Inside the cell, the radioactive cobalt encompassed a cylindrical sample chamber. The chamber was mobile and was elevated to the top of the cell for sample loading by manual control. Chamber operation can also be initiated by a timer which will automatically elevate the chamber after a preset irradiation time. An external view of the irradiator with the sample chamber in an elevated position is shown in Fig. 6.

The high temperature furnace: The LECO (Laboratory Equipment Corporation) model 540 resistance furnace, as shown in Fig. 7, provided the high temperature isothermal conditions required for the thermal decomposition of manganous and zinc carbonate. This furnace contained two combustion tubes and four silicon carbide heating elements; two elements were above the combustion tubes and two below. The temperature of the furnace was controlled by the voltage applied across the heating elements.

The voltage applied to the heating elements of the furnace ranged from 0 to 230 volts. A coarse control with six positions advanced the voltage approximately 38.5 volts per step and a fine control, also with six positions, added approximately 7.7 volts per step to the voltage of the coarse control. These controls provided regulation of the furnace temperature to a maximum temperature of 3000° F.

Fig. 6. External view of "Gammacell"-220 with a sample in the elevated irradiation chamber.

Fig. 7. A view of the LECO model 540 resistance furnace.

The temperature within the furnace was detected by a platinum, platinum-rhodium thermocouple which was placed in a special adapter to maintain a constant thermocouple position in the furnace. For this research, the thermocouple was connected to a Barber-Coleman 292P Capacitrol on-off type temperature controller. This controller automatically maintained the furnace temperature within $\pm$ 10° F of the set point.

The gas chromatography system: The gas chromatography system used was a Varian Aerograph 90P3 and matching model 30 strip chart recorder. This system was used to analyze quantitatively the gas swept out of the decomposition zone for the carbon dioxide gas released by thermal decomposition of manganous and zinc carbonate.

The main features of the gas chromatograph included a carrier gas, an adsorption column, and a detector. Temperature control of the column and detector were also provided. In this research, the carrier gas was helium; the chromatographic column was 4 ft. x 1/4 in. diameter copper tubing packed with 60/80 mesh silica gel. Gas analysis was performed with a thermal conductivity detector.

The strip chart recorder was restricted to 1 mV full scale and had four chart speeds. An attenuation control on the gas chromatograph was used to reduce excessively high output voltages to the recorder and thus bring them within the 1 mV range. Attenuation was by factors of 2, from settings of 1 to 512; thus relatively high voltage output signals could be recorded. A photograph of the gas chromatograph and the strip chart recorder is shown in Fig. 8.

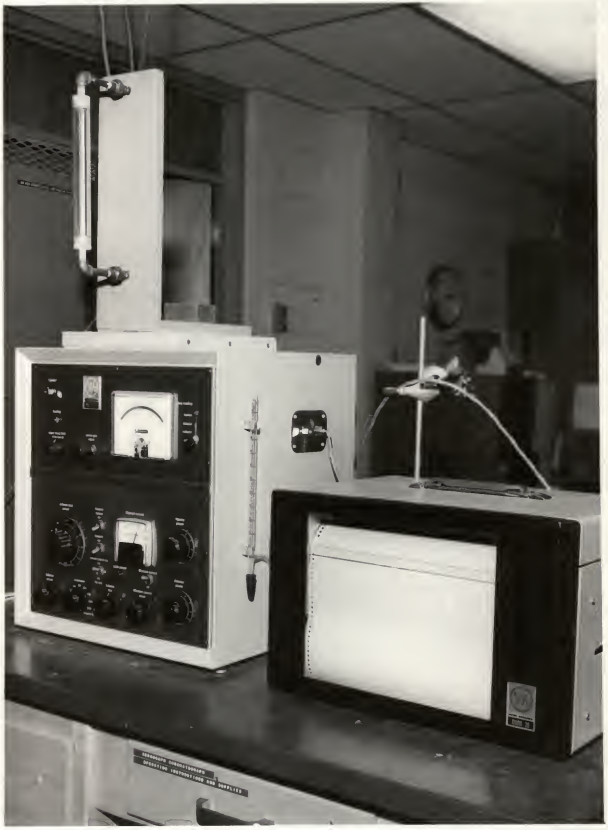

Fig. 8. A view of the 90P3 gas chromatograph and model 30 strip chart recorder.

4.0 EXPERIMENTAL PROCEDURE

Chemical reagent grade zinc and manganous carbonates were used in the experiments. Both carbonates were in powdered form and were filtered through a 200 mesh screen to remove any coarse particles. The powders were then stored in tightly stoppered bottles to reduce their decomposition at room temperature.

For each experiment a stainless steel boat was vibration packed with one of the carbonates until it was full. To obtain some uniformity in the packed powder, approximately the same weight of sample was added in each experiment. An attempt was also made to remove any adsorbed moisture from the samples by drying them in a dry air atmosphere through a procedure presented in Appendix A. After drying, the carbonates were kept in rubber stoppered glass vials until time for their thermal decomposition or for their irradiation in the "Gammacell."

Fig. 9 shows a diagram of the system used for the thermal decomposition of the carbonates. In each experiment a carbonate sample in its stainless steel boat was centered in the isothermal region of the high temperature furnace inside a stainless steel tube. The isothermal region was about the same length as the boats, 2.25 inches. The carbon dioxide released in the decomposition of the carbonate was carried from the stainless steel tube through copper tubing to the gas chromatograph by helium gas flowing at 4-5 ml/min. The injection system on the chromatograph was then used to divert approximately 1 cm^3 samples from the flowing stream into the chromatograph for carbon dioxide analysis at intervals of at least two minutes.

The operating conditions of the chromatograph were as follows:

Carrier gas - Helium

Carrier gas flow rate - 50 ml/min.

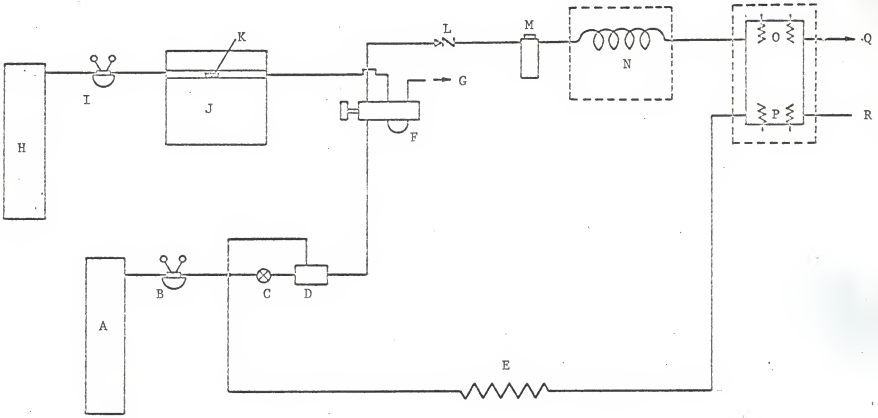

A. Helium Gas Tank
B. Reduction Valve
C. Needle Valve
D. Flow Controller
E. Reference Flow Restricter
F. lcc. Gas Sampling Valve
G. To RGI 1100 Flowmeter
H. Helium Gas Tank
I. Reduction Valve
J. High Temperature Furnace
K. Carbonate Sample
L. One-Way Check Valve
M. Syringe Injection Port
N. Silica Gel Column
O. Sensing Filaments
P. Reference Filaments
Q. To Bubble-Type Flowmeter
R. To Atmosphere

Fig. 9. Schematic diagram of thermal decomposition system.

Column temperature	- 290° F
Detector temperature	- 140° F
Filament current	- 200 mA

The chromatograph was absolutely calibrated for the quantitative measure of carbon dioxide gas in a helium-carbon dioxide gaseous mixture by a method presented in Appendix B.

The times of sample injections relative to the initial time of placement of the carbonate into the furnace, t = 0, were recorded so that the variance of the reaction rate with time could be observed. This procedure was followed for the range of decomposition temperatures 400-700° F as measured by the temperature controller of the furnace. To obtain a more precise measurement of the decomposition temperature, two alumel-chromel thermocouples were used to measure the temperature within the stainless steel tube and also its wall temperature at the position where the center of the decomposing carbonate was to be located. The temperature readings were then used to calculate the true gas temperature at which the carbonate was decomposing through an equation which corrects for thermocouple radiation error (Appendix C).

For comparison of unirradiated and irradiated zinc and manganous carbonates at various decomposition temperatures, the carbonates were subjected to a pre-irradiation in the "Gammacell" before thermal decomposition. In this procedure the carbonates were put into sealed 2 oz. polyethylene bottles after drying. The carbonates were then irradiated one at a time in the "Gammacell" in a plastic rack which was designed to center the carbonate within the irradiation chamber. After irradiation 1 cm^3 samplings of the atmosphere in the plastic bottles were taken with a 20 cm^3 gas tight syringe and injected into the chromatograph for analysis of the carbon dioxide con-

tent. For comparison, samplings were also taken of the atmospheres of unirradiated samples which had been enclosed in the polyethylene bottles for times equal to the irradiation times. The irradiated carbonates were then thermally decomposed in the same system and at the same temperatures used for the unirradiated carbonates.

5.0 PRESENTATION OF DATA

Powdered zinc carbonate was thermally decomposed at temperatures of 189, 242, and 292° C. Decompositions were also performed at the same temperatures for powders which had received a 9.45 Mrad absorbed dose in air from cobalt-60 gamma radiation prior to their decomposition. One additional sample was given 18.8 Mrad of gamma radiation prior to decomposition at 189° C.

During the decompositions the carbon dioxide content of the sample carrier gas (helium) was monitored (at injector temperature) at two minute intervals from the start of heating by the gas chromatograph. The chromatographic output was converted to mole percent of carbon dioxide using the absolute calibration curve of Appendix B. The mole content of carbon dioxide in the sample carrier gas was used to determine the rate of flow of the carbon dioxide, which was then put on a unit dried weight of powdered zinc carbonate basis to obtain the carbon dioxide production rate with time. Histograms of the carbon dioxide production rate with time for the decomposition temperatures of the powdered zinc carbonate are presented in Figs. 10-16.

Powdered manganous carbonate was treated in the same manner for decomposition temperatures of 242, 292, and 345° C. An additional sample was given an 18.8 Mrad gamma irradiation prior to decomposition at 929° C. The carbonate was also decomposed at 396° C for two different sample carrier gas rates of flow. Histograms of the carbon dioxide production rate at the decomposition temperatures of powdered manganous carbonates are presented in Figs. 17-26.

For further reference the carbon dioxide production rates as a function of time at the various decomposition temperatures noted above are presented in tabular form in Appendix E for both zinc and manganous carbonate.

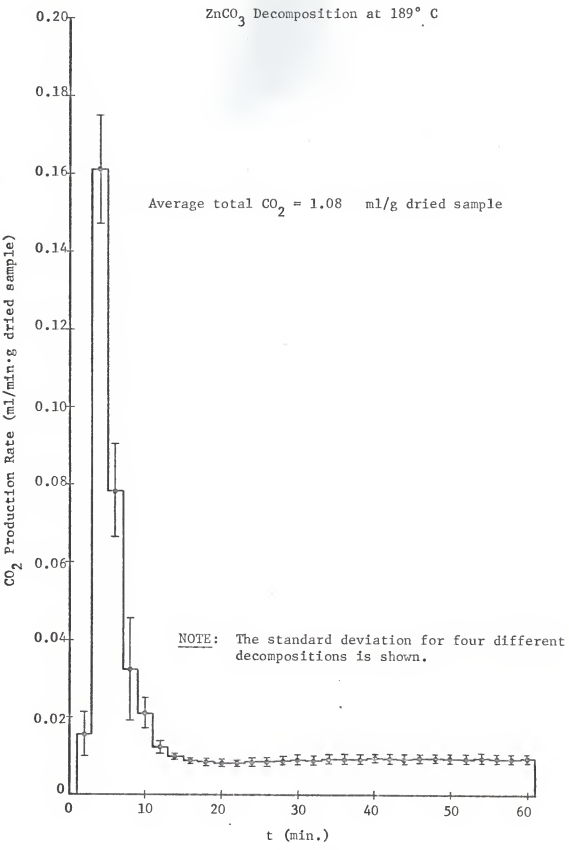

Fig. 10. CO_2 production rate with time for unirradiated $ZnCO_3$ powder at 189° C.

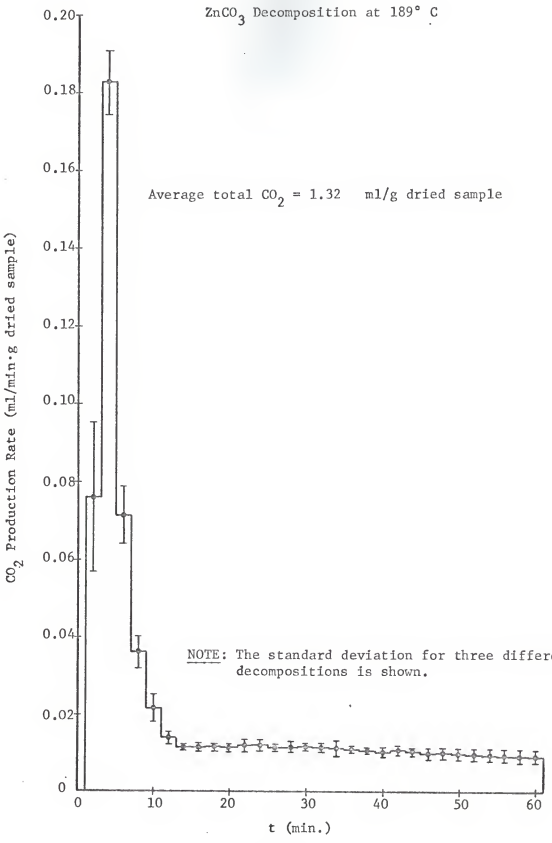

Fig. 11. CO_2 production rate with time for 9.45 Mrad pre-irradiated powdered $ZnCO_3$ at 189° C.

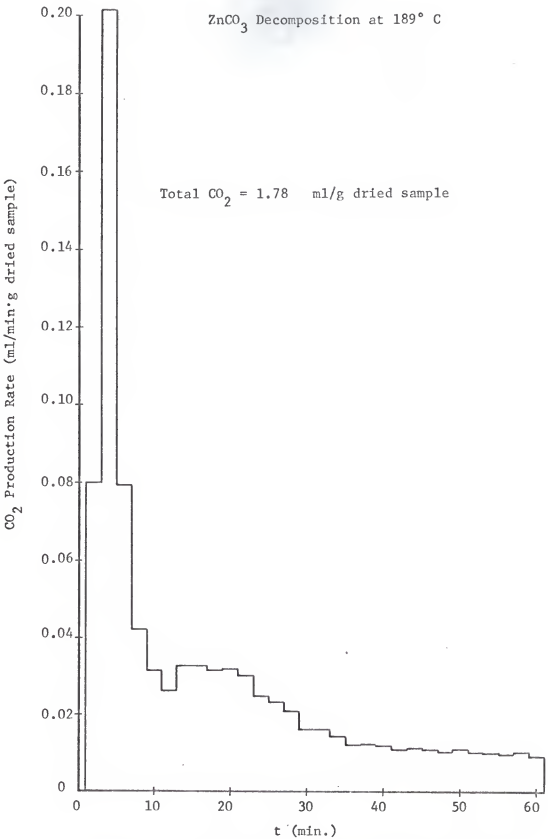

Fig. 12. CO_2 production rate with time for 18.8 Mrad pre-irradiated $ZnCO_3$ powder at 189° C.

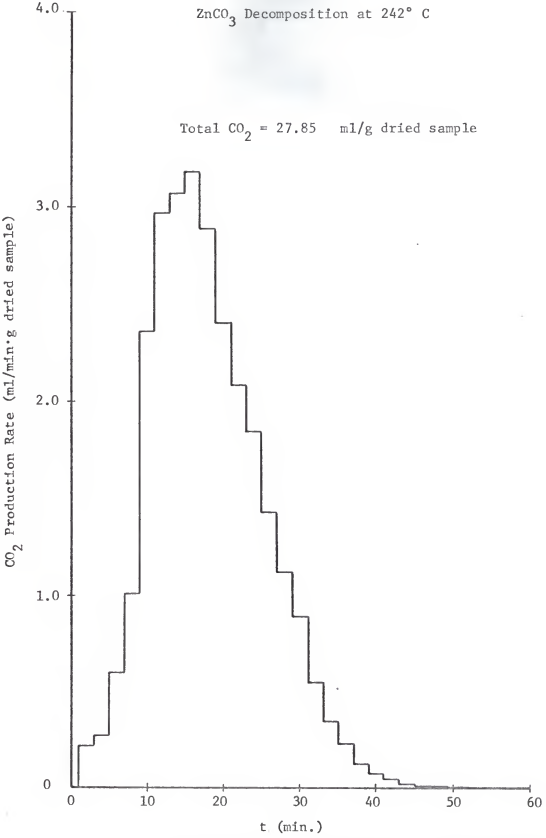

Fig. 13. CO_2 production rate with time for unirradiated $ZnCO_3$ powder at 242° C.

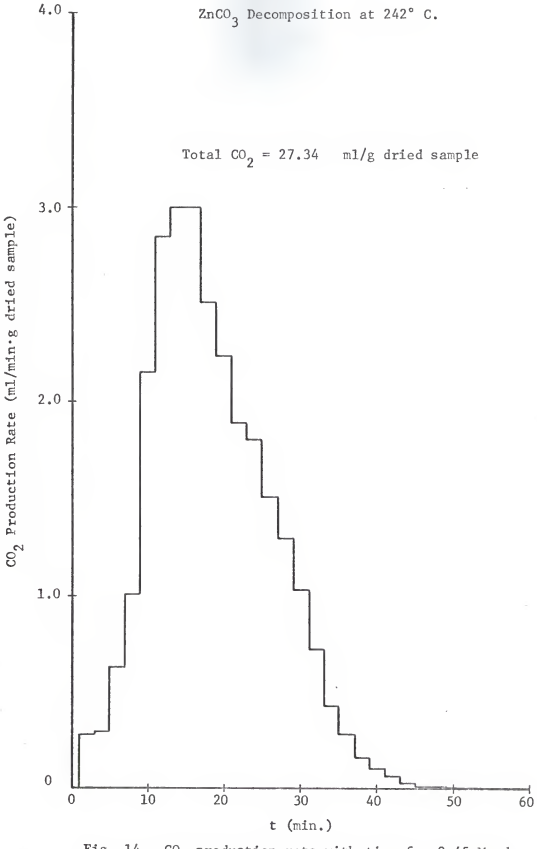

Fig. 14. CO_2 production rate with time for 9.45 Mrad pre-irradiated $ZnCO_3$ powder at 242° C.

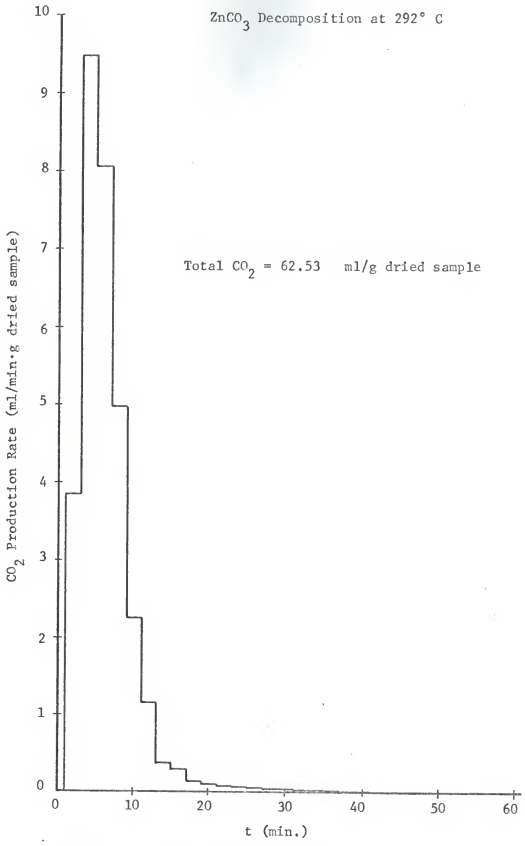

Fig. 15. CO_2 production rate with time for unirradiated $ZnCO_3$ powder at 292° C.

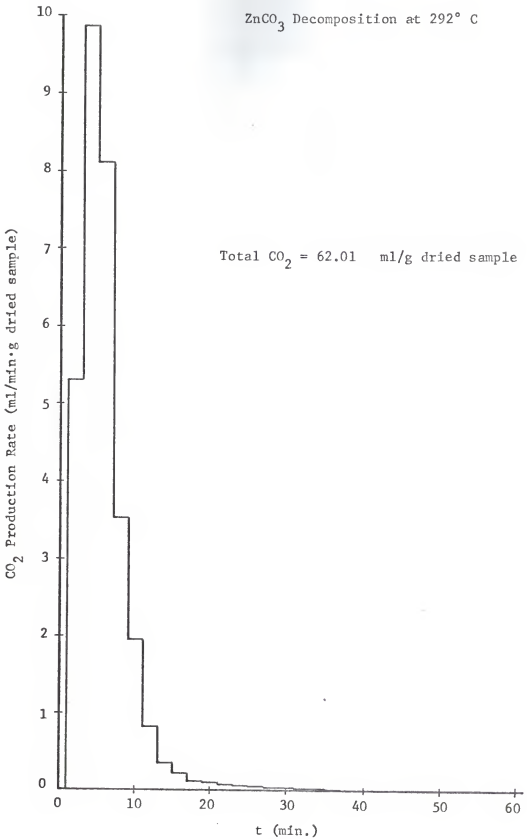

Fig. 16. CO_2 production rate with time for 9.45 Mrad pre-irradiated $ZnCO_3$ powder at 292° C.

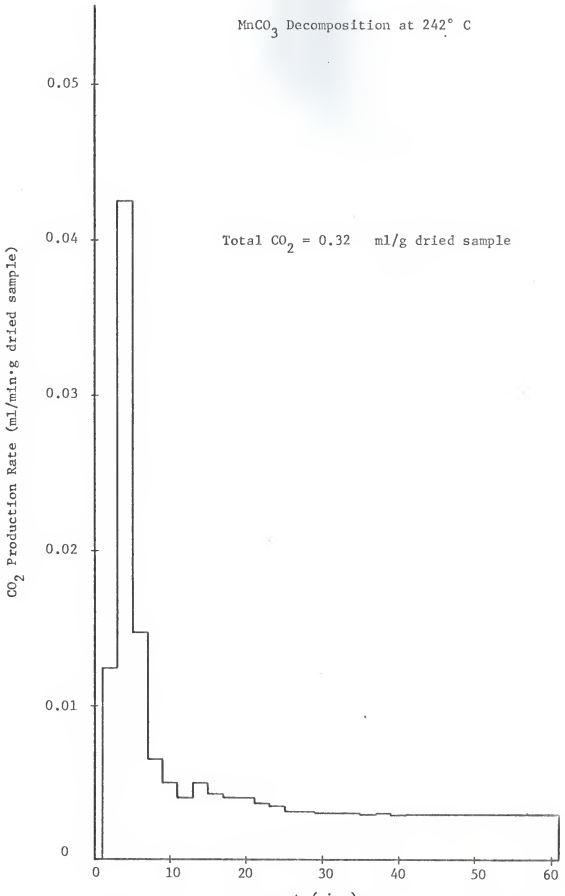

Fig. 17. CO_2 production rate with time for unirradiated $MnCO_3$ powder at 242° C.

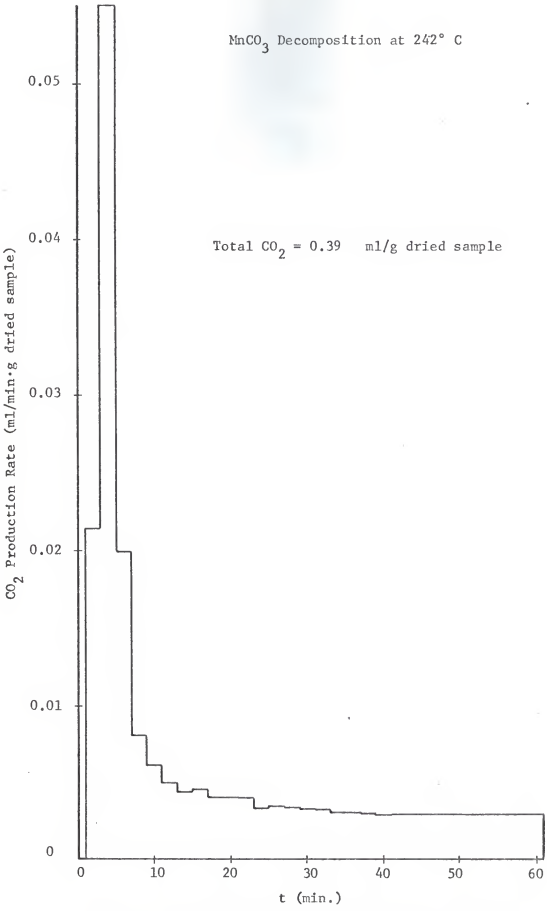

Fig. 18. CO_2 production rate with time for 9.45 Mrad pre-irradiated $MnCO_3$ powder at 242° C.

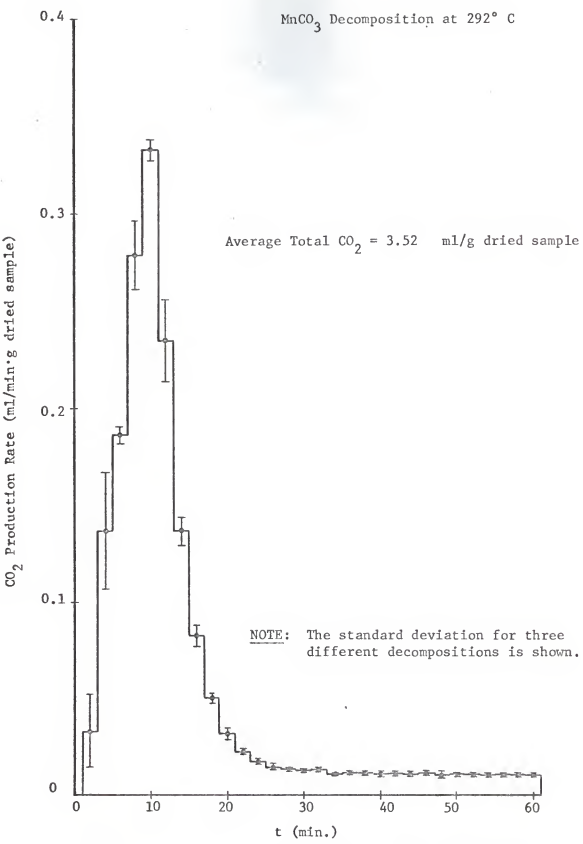

Fig. 19. CO_2 production rate with time for unirradiated $MnCO_3$ powder at 292° C.

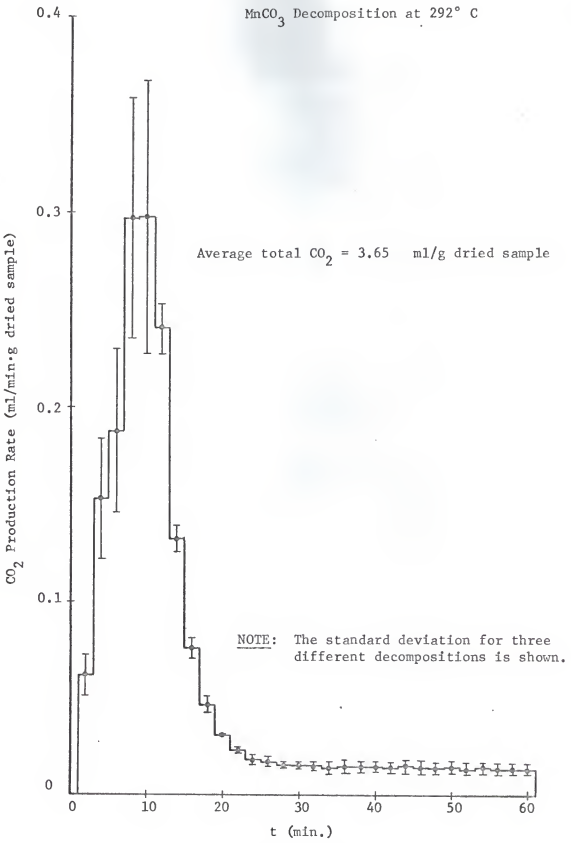

Fig. 20. CO_2 production rate with time for 9.45 Mrad pre-irradiated $MnCO_3$ powder at 292° C.

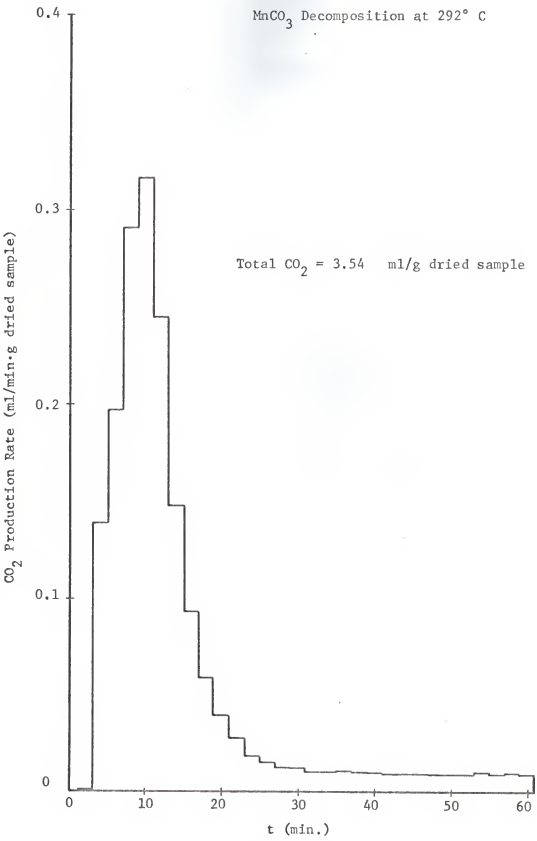

Fig. 21. CO_2 production rate with time for unirradiated $MnCO_3$ powder for comparison with 18.8 Mrad pre-irradiated $MnCO_3$ at 292° C.

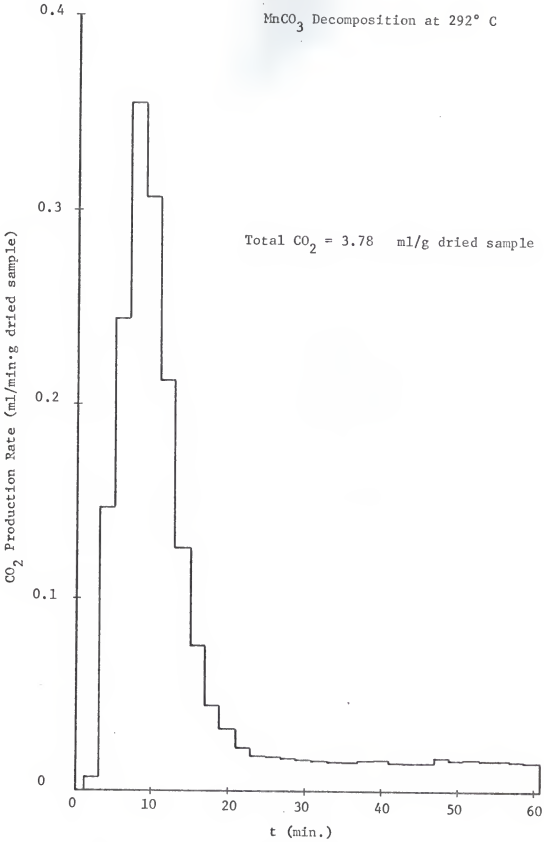

Fig. 22. CO_2 production rate with time for 18.8 Mrad pre-irradiated $MnCO_3$ powder at 292° C.

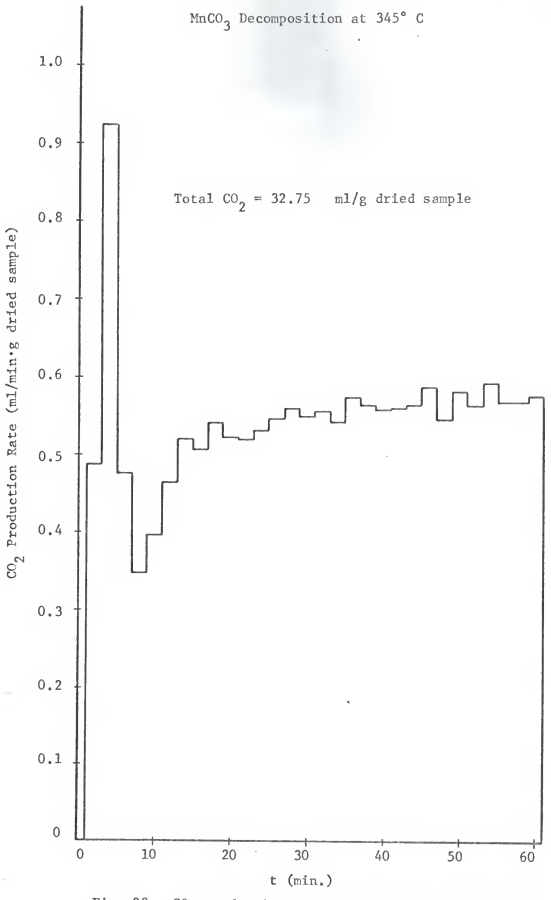

Fig. 23. CO_2 production rate with time for unirradiated $MnCO_3$ powder at 345° C.

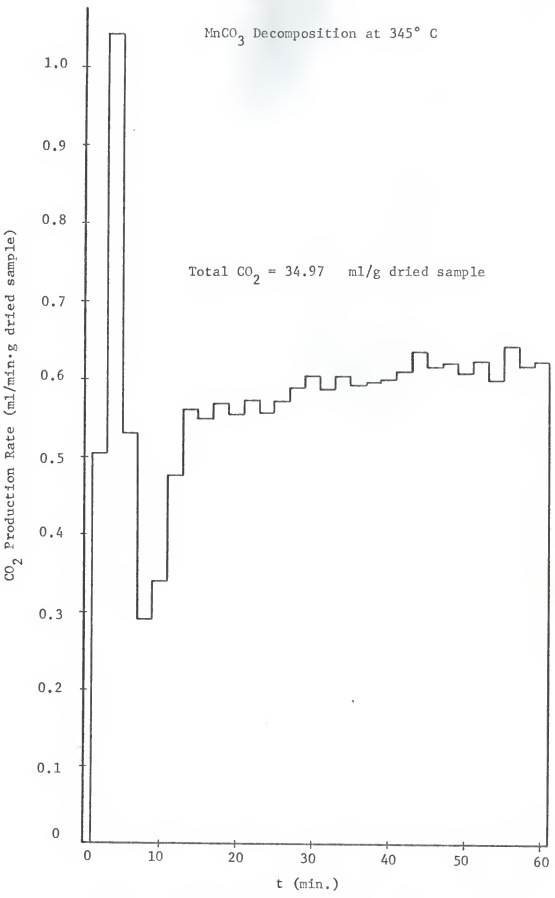

Fig. 24. CO_2 production rate with time for 9.45 Mrad pre-irradiated $MnCO_3$ powder at 345° C.

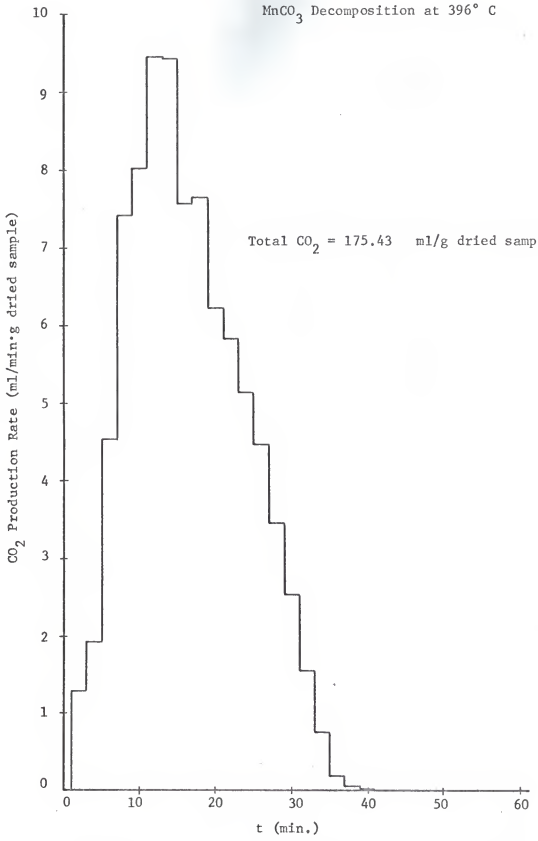

Fig. 25. CO_2 production rate with time for unirradiated $MnCO_3$ powder at 396° C with 4 ml/min helium flow rate.

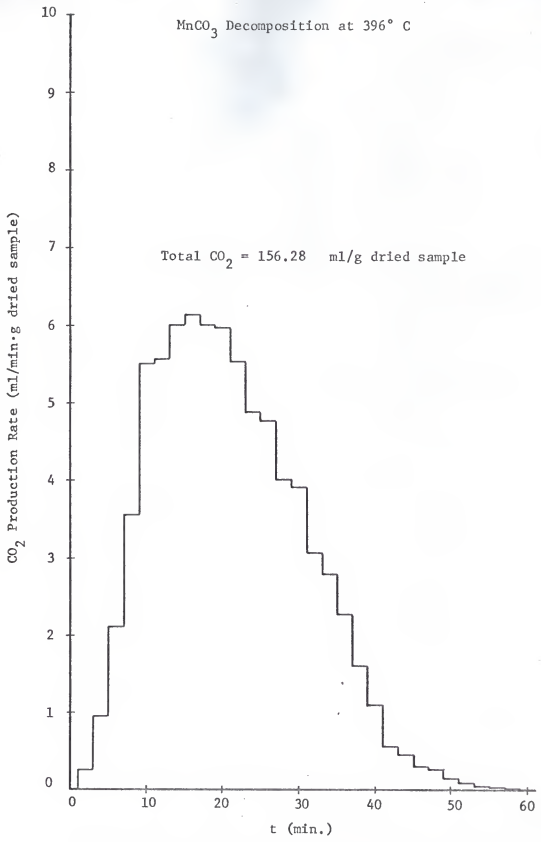

Fig. 26. CO_2 production rate with time for unirradiated $MnCO_3$ powder at 396° C with 1.3 ml/min helium flow rate.

6.0 DISCUSSION OF RESULTS

6.1 Analysis of the Data on Carbon Dioxide Production Rate

The histogram for the carbon dioxide production rate, as a function of time from the start of decomposition, were observed to have the same general form at all decomposition temperatures, i.e., a rapid rise to a maximum rate and then a gradual decline in rate. The rapid rise can be attributed to the initial mixing of the carbon dioxide in the helium carrier gas stream and to the rapid decomposition of the external surface of the powdered carbonate. In addition, the rapid rise occurred during the time interval in which the carbonates were reaching thermal equilibrium. For the range of decomposition temperatures used in this work, the carbonates were shown in Appendix D to reach thermal equilibrium in approximately six minutes from the start of heating. For the lower decomposition temperatures of the carbonates, the time of the rapid rise was similar to the time required for the carbonates to reach thermal equilibrium. It was further observed that the period of the rapid rise was extended beyond the period of transient heating within the carbonates for higher decomposition temperatures. The transient heating of the carbonates was not expected, however, to have a controlling influence on the reaction kinetics during the rapid rise. This conclusion was quite reasonable since the initial part of the decomposition of the carbonates occurred on or near their surface where the decomposition temperature was reached almost instantaneously during heating.

The gradual decline of the production rate with time designated either the retention of carbon dioxide within the carbonate or the approach to completion of the decomposition. The retention of carbon dioxide within the

carbonate will occur when the decomposition temperature is too low to promote rapid decomposition of the carbonate and/or rapid diffusion of carbon dioxide to the surface of the carbonate. Decomposed layers of metallic oxide also restrict diffusion of carbon dioxide since the decomposition will proceed from the adsorption surface of the powdered carbonate into the carbonate particles. The oxide may also retard the carbon dioxide long enough for recombination to occur. That increased temperature was effective in increasing carbon dioxide production for equal periods of decomposition was shown by the increase in the area of the histograms with temperature.

Furthermore, for decompositions of powdered carbonate mixed with an inert dispersing material present, the total weight lost during the decomposition per unit weight of dried carbonate was approximately the same as for carbonate samples which contained no inert dispersant material. Since the inert material was not effective in releasing more carbon dioxide from the packed carbonate, it can be concluded that the diffusion of the carbon dioxide was not controlled by sintering or other obstructions of the pores between the carbonate powder particles. Any diffusion control of the carbon dioxide evolution was, therefore, concluded to come from within the carbonate particles.

Over the one hour period for which the decompositions were observed, the production rates never declined toward zero, except for temperatures which were high enough to promote complete decomposition within that time span. Instead, the production rates usually approached a constant value. In the case of powdered manganous carbonate at 345° C, the production rate, after passing a maximum, declined and then rose again to a constant decomposition rate. It was suspected that back-mixing of carbon dioxide in the helium

carrier gas and diffusion of carbon dioxide from the carbonate caused these effects.

Changing the sample carrier gas (helium) rate of flow was observed to affect the carbon dioxide production rate with decomposition time as shown in Figs. 25-26. The total carbon dioxide production over the same decomposition period was much greater for the higher rate of flow. It was concluded that the increased rate of flow was flushing more carbon dioxide from the powdered carbonate, thus forcing the equilibrium for the reaction toward greater carbon dioxide production.

The carbon dioxide production was expected to be proportional to the dry carbonate weight at each decomposition temperature. For this reason, the carbon dioxide production rate was expressed on a basis of unit dried weight of carbonate. This basis was useful since the decomposition vessels were easily packed by volume rather than by weight. Using this expression of the production rate, the total carbon dioxide per unit weight of carbonate at each decomposition temperature was expected to be fairly constant over equivalent decomposition periods. The results of several decompositions for unirradiated and irradiated zinc carbonate at 189° C and manganous carbonate at 292° C showed that the total carbon dioxide production per unit weight of carbonate varied from 3 - 12% of their average values. This deviation was concluded to represent non-uniformity in vibration packing the carbonate samples and in the composition and size of the carbonate particles.

6.2 Observable Effects of Gamma Radiation Damage

Powdered zinc and manganous carbonate which had received some preirradiation, in general, showed increases in carbon dioxide production rate

during the first ten minutes of their decomposition over carbonates not receiving any radiation treatment. For some decomposition temperatures an increase in production rate also occurred in the region where the production rate approached a constant value. These effects became more apparent with increased gamma radiation dose.

The initial increase in the production rate for pre-irradiated carbonates was so rapid that it was concluded to be caused by energy deposition from the gamma radiation which ruptured the bonding between the carbon dioxide and the metallic oxide and weakened the carbonate structure by the creation of point defects on or near the surface of the carbonate. The increase in the production rate at later times was likely an observance of this same type of radiation damage but which was diffusion-controlled within the carbonate particles.

The carbon dioxide yields of pre-irradiated carbonates were found to be statistically greater than those for unirradiated carbonates at low decomposition temperatures. That the total carbon dioxide production over equal decomposition periods appeared to increase with gamma radiation dose is shown graphically in Fig. 27 for zinc and manganous carbonate at decomposition temperatures of 189° C and 292° C, respectively. The rising trend of the data is shown by the least squares linear fit of the three data points.

From the samplings of the air atmospheres in the polyethylene bottles in which the carbonate samples were irradiated appeared that chromatographic analysis showed small quantities of carbon dioxide and traces of carbon monoxide while samplings from unirradiated carbonate samples which were enclosed in the polyethylene bottles for times equivalent to the irradiation times showed only traces of carbon dioxide. Samplings taken from empty poly-

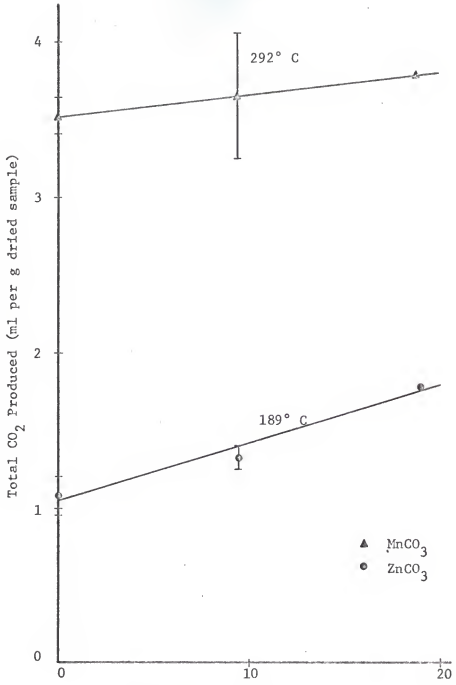

Fig. 27. The effect on the total carbon dioxide production of powdered zinc and manganous carbonate of gamma irradiation prior to thermal decomposition.

ethylene bottles after they had received the same radiation exposure as used in irradiation of the carbonate samples also seemed to show quantities of carbon dioxide comparable to that found in the atmospheres of the irradiated carbonates.

The work of Dole on irradiated polyethylene (40) revealed that carbon dioxide was not a by-product of irradiated polyethylene. Dole's analysis with the mass spectrometer of irradiated polyethylene atmospheres showed large quantities of hydrogen and trace amounts of low molecular weight hydrocarbons. If one of the hydrocarbon forms released from irradiated polyethylene had the same retention time in the chromatograph as carbon dioxide this could explain the observed effect.

At the time of this research, a mass spectrometer was not available for further study of the atmospheres in the polyethylene bottles. Thus, no conclusions can be drawn as to the extent of CO_2 production during irradiation.

6.3 Problems Encountered in Analyzing the Thermal Decompositions

To study the thermal decomposition kinetics of powdered zinc and manganous carbonate in terms of the fraction of a sample decomposed a material balance was necessary. A balance was made between the amount of carbonate decomposed and the carbon dioxide produced in the decomposition as determined by the change in weight of the sample. This result was compared with the volume of carbon dioxide measured by the gas chromatograph. Using the assumption that the powdered carbonates were pure in form, a material balance could not be obtained for any of the decomposition data. In an attempt to reconcile the discrepancy an analysis of the carbonates for water and metallic oxide content was undertaken. The carbonates were not expected to contain any other appreciable impurities.

Although a Karl Fischer titration test for water was attempted for the zinc carbonate, this test could not be used for manganous carbonate because of its insolubility in common organic solvents. Although the test detected a large fraction of water in the zinc carbonate, it was inconclusive because the expiration date on the Karl Fischer reagent had passed, and the zinc carbonate was not completely soluble in any of the organic solvents used. The insoluble nature of the zinc and manganous carbonate in organic solvents also prevented the use of nuclear magnetic resonance for the water determination.

Since no other means were available for analysis of the carbonates, samples were sent to Galbraith Laboratories, Knoxville, Tennessee for determination of carbon and hydrogen content. The results of their analysis for two replications are presented in Table I. Also given is the carbon content which was calculated for the carbonates after correcting for the water content. The water content was computed from the percent hydrogen furnished by Galbraith Laboratories.

Table I. The Analysis of Powdered Zinc and Manganous Carbonate for Hydrogen and Carbon Content on a Weight Percent Basis by Galbraith Laboratories.

	% Hydrogen	Average % Hydrogen	% Carbon	Average % Carbon	% Carbon in Carbonate after water correction
$ZnCO_3$	1.41 1.35	1.38	4.94 5.15	5.045	8.39
$MnCO_3$	0.31 0.29	0.30	10.21 10.31	10.26	10.17

The presence of hydrogen showed that the carbonates contained water. The water content of the experimental samples when computed from the hydrogen content reported by Galbraith Laboratories greatly exceeded the water removed from the carbonates by the drying apparatus of Appendix A. The analysis from Galbraith Laboratories also showed that zinc carbonate was partially decomposed while the manganous carbonate was not.

The analysis from Galbraith Laboratories was used in checking for the decompositions of unirradiated zinc and manganous carbonate at 292° C and 396° C, respectively (the decomposition of these particular samples appeared to most nearly approach completion). Assuming that all the water was driven from the samples at these temperatures, the carbon dioxide losses were computed from the approximate weights lost by the carbonates during their decomposition. For comparison, the results of these calculations are presented in Table II.

Table II. The Results of a Material Balance on Powdered Zinc and Manganous Carbonate after Correcting for Water and Decomposed Material.

	Decomposition Temperature (°C)	Sample Weight (g)	Maximum CO_2 Sample Can Generate (ml)	Approximate CO_2 Lost* (ml)	CO_2 Measured (ml)
$ZnCO_3$	292	1.1024	103.73	82.30	68.02
$MnCO_3$	396	1.2071	231.01	213.26	211.17

*Based on change in sample weight.

From the above data it can be concluded that the powdered zinc and manganous carbonate showed a retention for carbon dioxide at their decomposi-

tion temperatures. They, likewise, lost more carbon dioxide than was measured by the gas chromatograph. The large difference between the carbon dioxide lost and the carbon dioxide measured for the zinc carbonate suggested that perhaps other impurities were present in the compound. The good agreement in these values for manganous carbonate indicated that this compound contained no other impurities. Further chemical analysis of the zinc carbonate was not attempted in this research.

The large initial decomposition rates of the zinc and manganous carbonate suggested that some carbon dioxide might have escaped from the decomposition system during the time interval in which the carbonate sample was placed in the high temperature furnace and the helium carrier gas line was resealed. An attempt was made to determine if any appreciable loss had occurred by thermally decomposing zinc and manganous carbonate samples starting at room temperature. (The carbonate sample was placed in the furnace at room temperature where no decomposition would occur; the decomposition chamber was sealed and then heating of the furnace to "red heat" was started.) This test showed that it was necessary to approach "red heat" temperatures, approximately 1300° F, before all the carbon dioxide was driven from the carbonates. The results of the test are presented in Table III.

Table III. The Carbon Dioxide Measured on Heating Carbonate Samples from Room Temperature.

	Sample Weight (g)	Maximum CO_2 Sample Can Generate (ml)	Approximate CO_2 Lost* (ml)	CO_2 Measured (ml)
$ZnCO_3$	0.8861	82.62	64.95	58.20
$MnCO_3$	1.2475	238.74	231.38	203.56

*Based on change in sample weight.

By heating to red heat a reduction in the carbon dioxide retention was found for both carbonates; however, the carbon dioxide lost during the decomposition was still greater than the carbon dioxide measured by the chromatograph. The impurity content of the zinc carbonate would again account for its low carbon dioxide measurement. On the other hand, the low carbon dioxide measurement for the manganous carbonate would imply that there are certain inherent errors in the analysis of the decompositions and this particular experiment helped to delineate some of them.

Likely sources of error in the determination of the measured carbon dioxide were in the calibration curves for the gas chromatograph and the gas flowmeter. Several points on the gas chromatograph calibration curve were rechecked after the decomposition data were completed. The calibration was found to compare within the statistics of the original calibration. There also existed the possibility that the furnace temperature would have an unforeseen effect on the chromatograph calibration which would account for the error in the carbon dioxide measurements previously cited. Therefore, a flow line was passed through the high temperature furnace, which was at 396° C, to the gas chromatograph. Several calibration points were then checked by passing helium-carbon dioxide gas streams of known concentration through the line and analyzing the gases with the gas chromatograph. The calibration was again found to compare within the statistics of the original calibration.

The F1100 gas flowmeter was calibrated according to the design equations and air calibration furnished by the manufacturer. The calibration curves obtained for helium and carbon dioxide were therefore assumed to be quite accurate. The loss of accuracy in the flowmeter was thus attributed to human error in reading the flowmeter. This error was estimated to be $\pm$ 0.25 of a

division on the flowmeter scale. From the calibration curves for helium and carbon dioxide, the error in the flow rates was then found to be less than 5% for flow rates greater than 4 ml/min and as much as 15% for flow rates less than 4 ml/min. There was no means of further assessing the accuracy of the flowmeter readings which could very well have been affected by condensation within the flowmeter from water liberated from the carbonates.

The loss of carbon dioxide around the O-ring seals of the chromatograph injection system was also suspected since traces of air were found in every sampling analyzed by the chromatograph.

6.4 Analysis of the Kinetics of Thermal Decomposition for Powdered Zinc and Manganous Carbonate

In making this study of the kinetics of thermal decomposition for powdered zinc and manganous carbonate, the chemical analysis of the carbonates by Galbraith Laboratories was assumed to be valid and the carbon dioxide measured by the chromatograph was assumed to be a true indication of the carbon dioxide released by the decomposed carbonate.

The thermal decomposition curve for the powdered zinc carbonate at 292° C is presented in Fig. 28. On comparison of this curve with the generalized decomposition curve (Fig. 1), the decay period was found to cover the majority of the decomposition. Effect of retention of carbon dioxide within the packed zinc carbonate powder was shown by the very slow rise in the decomposition curve after the carbonate was 65% decomposed. The decomposition was further examined for first order reaction kinetics by plotting $-\ln(1-\alpha)$ against time. This curve as presented in Fig. 29 showed a linear region from 2 to 8 minutes after the start of decomposition, which indicated a first order reaction in this time interval. The fact that an extrapolation

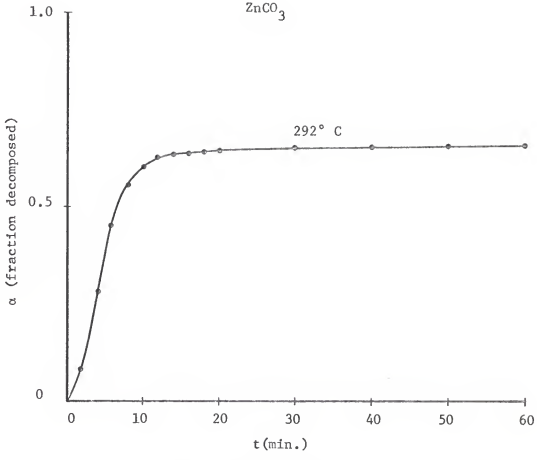

Fig. 28. Thermal decomposition curve for vibration-packed $ZnCO_3$ powder at 292° C.

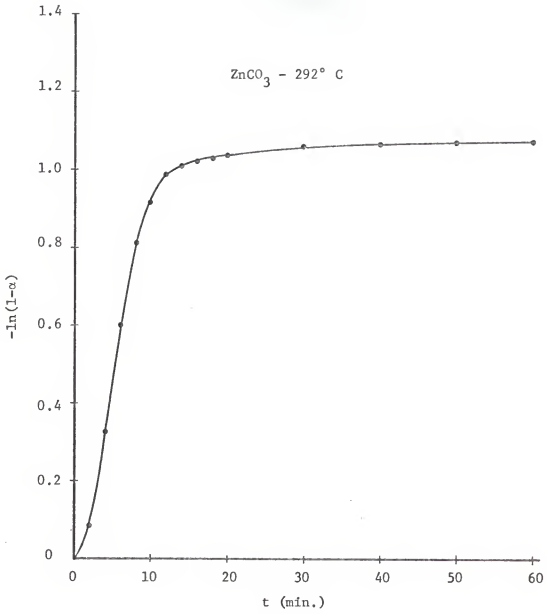

Fig. 29. The thermal decomposition of $ZnCO_3$ at 292° C, showing that initially the reaction is governed by first order kinetics.

of the linear region did not pass through the origin was an indication of the finite time required to heat the sample to equilibrium temperature. Beyond 8 minutes the reaction kinetics became more complex. The reaction rate declined rapidly and was concluded to be diffusion-controlled.

Thermal decomposition curves for powdered manganous carbonate are plotted in Fig. 30 for various temperatures. A comparison of these curves with those of Razouk (Fig. 2) showed that the decomposition of the powdered carbonate used in this work did not approach the decompositions for his precipitated carbonate, except at the uppermost decomposition temperature of 396° C. The slow rise of the thermal decomposition curves obtained in this work most probably resulted from the method of packing the carbonates and the particle size of the carbonate. The water contained within the carbonate could also have affected this slow rise by impeding the diffusion of the carbon dioxide from the carbonate. In summary the physical characteristics of a particular sample greatly affect the decomposition behavior.

The decomposition of manganous carbonate was also examined for first order reaction kinetics. A plot of $-\ln(1-\alpha)$ against time for the decomposition at 396° C is shown in Fig. 31. From the shape of the curve it was evident that a first order reaction did not occur. Instead, its sigmoidal shape was more characteristic of the adsorption-desorption effect for gases diffusing through particulate matter. It was thus concluded that the decomposition of the powdered manganous carbonate was a diffusion limited situation.

The kinetics of the decomposition was further examined by plotting $(w/w_o)^{1/3}$ against time for decompositions at 345 and 396° C. The majority of the data was fitted linearly as shown in Fig. 32. The major portion of the decomposition was therefore governed by the one-third power law of con-

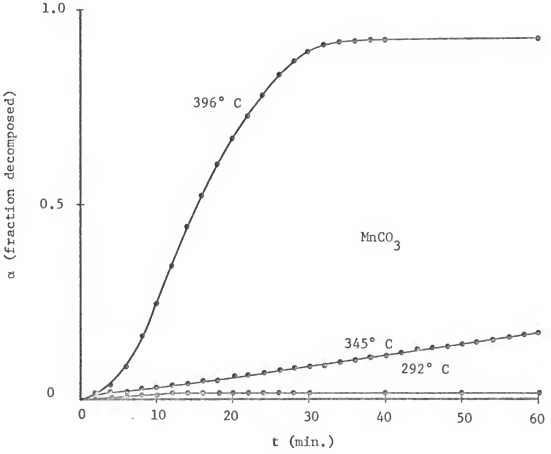

Fig. 30. Thermal decomposition curves for vibration-packed $MnCO_3$ powder at various temperatures.

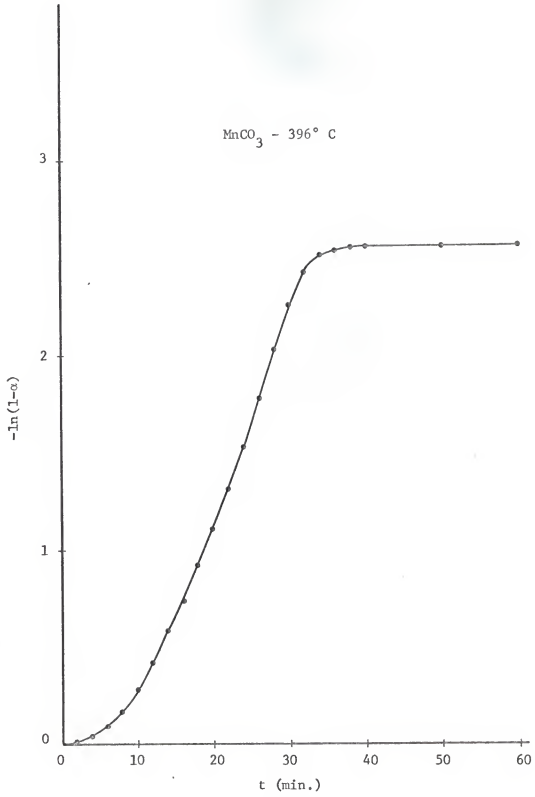

Fig. 31. The thermal decomposition of $MnCO_3$ at 396° C, showing that a first order reaction does not occur.

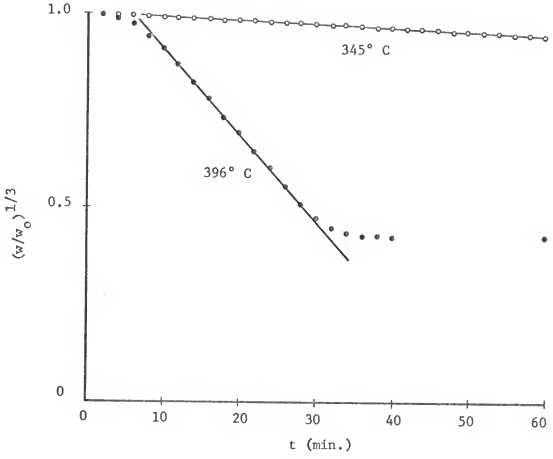

Fig. 32. Plots of $(w/w_o)^{1/3}$ against time, for thermal decomposition of vibration-packed $MnCO_3$ powder at different temperatures.

tracting spheres (see work of Razouk, Eq. 6). The kinetics of the decomposition of manganous carbonate were thus found to be in agreement with the findings of Razouk for his precipitated carbonate (Fig. 4).

7.0 SUMMARY OF CONCLUSIONS

The thermal decomposition of powdered zinc and manganous carbonate was successfully observed in this research using gas-solid chromatography for detection of the released carbon dioxide gas. The reaction rates for the decompositions were influenced by changes in decomposition temperature and the helium rate of flow over the carbonate samples. It was also concluded that the method of sample preparation, particle size, and impurity content of the carbonates influenced the reaction kinetics.

The carbonates were not fully decomposed in a reasonable period of time at any of the decomposition temperatures which were used in this research. Since dispersion of the carbonate powder with inert material did not increase the carbon dioxide production, the retention of the carbon dioxide was concluded to come from diffusion control within the carbonate particles.

Pre-irradiation of the carbonates with Cobalt-60 gamma rays in general increased the reaction rate during the early stages of the decomposition. Increases in the reaction rate during the final stages of decomposition were also observed at some temperatures. The latter effect was likely an observance of carbon dioxide produced by radiation damage which was diffusion controlled within the carbonate particles. In addition, carbon dioxide yields of the pre-irradiated carbonates were found to increase with gamma radiation dose over equal periods of decompositions. Although no direct evidence was found to support any mechanism of radiation damage, ruptured bonding and the creation of point defects were considered to be the major sources of radiation damage within the carbonates according to the present knowledge of gamma radiation damage in crystalline solids.

The analysis of gas samples from the environment of the closed polyethylene bottles in which the carbonates were irradiated was inconclusive. The gases produced by gamma irradiation of the polyethylene bottles resulted in what appeared to be a carbon dioxide peak when they were analyzed with the gas chromatograph. This peak masked the detection of any carbon dioxide which was liberated from the carbonates by gamma radiation.

The decomposition of the powdered zinc carbonate was shown to be governed by first order kinetics in its early stages, eventually becoming a diffusion-limited process. The manganous carbonate was shown to have a diffusion-controlled decomposition. The major portion of its decomposition was governed by the one-third power law of contracting spheres.

8.0 SUGGESTIONS FOR FURTHER STUDY

Severe time limitations were placed on the extent of this work by the amount of chromatographic output that could be analyzed by the cutting and weighing integration technique. The addition of an electronic digital integrator to the chromatographic system is highly recommended in further studies to permit more rapid chromatograph integration while maintaining the precision obtained by the cutting and weighing technique.

Since this research as noted earlier was limited in scope, it provided only an initial familiarization with the thermal decomposition apparatus employed and with gamma radiation effects on the thermal decomposition of manganous and zinc carbonate. This work should be extended to a more in-depth study. In particular, the effects of sample gas flow rate, particle size and total amounts of carbonate samples, higher gamma radiation doses, and recombination and radiation annealing should be given further study and consideration. The decomposition effects of other types of radiation including reactor gammas and neutrons as well as other high energy particles should be studied. More accurate methods of absolutely calibrating the gas chromatograph merit exploration, too.

The thermal decomposition apparatus and method could also be used to study the decomposition kinetics of other carbonate compounds. An additional study might include the quantitative and qualitative measure of gases released from heated and/or irradiated concrete mixtures. Such measurements would provide a direct means of evaluating temperature and radiation effects on this material.

9.0 ACKNOWLEDGEMENT

The writer takes this opportunity to express his deepest appreciation to Dr. Walter Meyer for his guidance as faculty adviser throughout the course of this work. Sincere thanks are offered to the Nuclear Engineering faculty and staff and Dr. Herbert Moser for their helpfulness in the performance of this research, to Miss Shirley Wilson for typing the thesis, and to his wife, Nancy, for her encouragement and invaluable assistance. The writer also expresses his sincere appreciation to the Atomic Energy Commission for supporting his studies at Kansas State University.

10.0 REFERENCES

1. G. Hennig, R. Lees and M. S. Matheson, "The Decomposition of Nitrate Crystals by Ionizing Radiations," J. Chem. Phys. 21, 664-8 (1953).

2. E. R. Johnson, "Radiation Induced Decomposition of Lead Nitrate," J. Am. Chem. Soc. 80, 4460-2 (1961).

3. E. R. Johnson and J. Forten, "Radiation-Induced Decomposition of Inorganic Nitrates," Discussions Faraday Soc., 31, 238-61 (1961).

4. C. J. Hochonadel and T. W. Davis, "Radiolysis of Solid Nitrates," J. Chem. Phys. 27, 333-4 (1957).

5. E. G. Prout, "The Thermal Decomposition of Irradiated Potassium Permanganate," J. Inorg. Nuclear Chem. 7, 368-77 (1958).

6. V. V. Boldyrev and A. N. Oblivantsev, "Effect of Preirradiation on the Thermal Decomposition of Permanganates of Group I of the Periodic System," Dokl. Akad. Nauk SSSR 150, 826-28 (1963).

7. J. Jach, "The Thermal Decomposition of $NaBrO_3$; Part II-Irradiated Material," J. Phys. Chem. Solids 24, 75-84 (1962).

8. J. Jach, "Thermal Decomposition of Irradiated α-Lead Azide," Trans. Faraday Soc. 59, 947-58 (1963).

9. R. M. Haynes and D. A. Young, "Thermal Decomposition of Silver Oxalate," Discussions Faraday Soc., 31, 229-37 (1961).

10. P. J. Herley and E. G. Prout, "Thermal Decomposition of Irradiated Lead Oxalate," Nature 184, Supply No. 7, 445-6 (1959).

11. E. P. Hyatt, I. B. Cutler and M. E. Wadsworth, "Calcium Carbonate Decomposition in Carbon Dioxide Atmosphere," J. Am. Ceram. Soc. 41, 70-4 (1958).

12. M. R. Lorenz and G. J. Janz, "A Dynamic Method for Measuring Dissociation Pressures," J. Chem. Educ. 40 (11), 611-12 (1963).

13. W. L. Wanmaker and D. Radiclovic, "The Dependence of the Rate of the Dissociation of Strontium Carbonate in Some Mixtures on Particle Size and Composition," Reactivity of Solids, edited by G. M. Schwab, Elsevier Publishing Company, New York, 533-4 (1965).

14. R. I. Razouk, R. Sh. Mikhail and G. M. Habashy, "The Thermal Decomposition of Manganous Carbonate," Egypt. J. Chem. 1, No. 2, 223-34 (1958).

15. M. J. Zawadzki and M. W. Szamborska, "Kinetics of the Decomposition of $ZnCO_3$," Bull. Intern. Acad. Polon. Sci., Classe Sci. Math. Nat., Ser. A, 27-31 (1948).

16. S. R. Mohanty and M. N. Ray, "Thermal Decomposition of Irradiated Manganese Carbonate," Proc. Nucl. Radiation Symp., Bombay 1964, 112-17 (1965).

17. A. K. Biswas and G. R. Bashforth, The Physical Chemistry of Metallurgical Processes, 43 (1962).

18. M. J. Zawadzki, "The Action of Gaseous Acidic Oxides on Solid Metal Oxides. The Decomposition of Carbonates, Sulfates, and Sulfites.," Festsku., edited by J. Arvid Hedvall, 611-34 (1948).

19. D. A. Young, "Decomposition of Solids," The International Encyclopedia of Physical Chemistry and Chemical Physics, 1-4 (1966).

20. J. Langmuir, "The Dissociation of Solids and the Kinetic Interpretation of the Phase Rule," J. Am. Chem. Soc. 38, 2263-7 (1916).

21. C. N. Hinshelwood and E. J. Bowen, "The Influence of Physical Conditions on the Velocity of Decomposition of Certain Crystalline Solids," Proc. Roy. Soc. A99, 203-12 (1921).

22. J. Y. MacDonald and C. N. Hinshelwood, "Formation and Growth of Silver Nuclei in the Decomposition of Silver Oxalate," J. Chem. Soc. 127, 2764-71 (1925).

23. S. Roginskii and E. Schultz, "Catalytic Processes in Solid Phase. I. Decomposition of Potassium Permanganate," Z. Physik. Chem. A138, 21-41 (1928).

24. V. Kohlschütter and M. Lüthi, "Investigations of the Principles of the Genetic Formation of Substances. II. The Course of Chemical Reaction in Crystals. 1. Experiments on Copper Compounds," Helv. Chim. Acta 13, 978-1006 (1930).

25. W. E. Garner et. al., "The Dehydration of Ammonium, Potassium and Some Mixed Alums," Proc. Roy. Soc. A189, 508-27 (1947).

26. W. E. Garner and H. V. Pike, "Dehydration Nuclei on Crystals of Copper Sulfate Pentahydrate," J. Chem. Soc. 1565-8 (1937).

27. W. E. Garner and J. A. Cooper, "Dehydration of Crystals of Chrome Alum," Proc. Roy. Soc. A174, 487-503 (1940).

28. B. Topley and M. L. Smith, "Kinetics of Salt-Hydrate Dissociations: $MnC_2O_4 \cdot 2H_2O = MnC_2O_4 + 2H_2O$," J. Chem. Soc., 321-5 (1935).

29. S. Roginskii and E. Schultz, "The Decomposition of Explosives at Low Temperatures," Phys. Zeit. der Sowjetunion 1, 679-99 (1932).

30. F. von Göler and G. Sachs, "The Kinetics of the Process of Crystallization," Z. Physik 77, 281-6 (1932).

31. S. V. Ismailov, "The Theory of Topochemical Reactions," Phys. Zeit. der Sowjetunion 4, 835-42 (1933).

32. M. Avrami, "Kinetics of Phase Change. I, II, and III," J. Chem. Phys. 7, 1103-12 (1939); 8, 212-24 (1940); 9, 177-84 (1941).

33. B. V. Erofeev, "Generalized Equation of Chemical Kinetics and Its Application in Reactions Involving Solids," Compt. Rend. Acad. Sci. URSS 52, 511-14 (1946).

34. K. L. Mampel, "Time vs. Amount of Reaction Formulas for Heterogeneous Reactions at the Phase Boundaries of Solids. I. and II.," Z. Physik. Chem. A187, 43-57, 235-49 (1940).

35. O. Levenspiel, Chemical Reaction Engineering, John Wiley & Sons, Inc., New York, 348-50 (1962).

36. F. Seitz, "Color Centers in Alkali Halide Crystals," Rev. Mod. Phys. 18, 384-408 (1946).

37. J. H. O. Varley, "A Mechanism for the Displacement of Ions in an Ionic Lattice," Nature 174, 886-7 (1954).

38. G. J. Dienes and G. H. Vineyard, Radiation Effects in Solids, Vol. II. (1957).

39. J. Jach, "Thermal Decomposition at Defects," Reactivity of Solids, edited by G. M. Schwab, Elsevier Publishing Company, New York, 422-31 (1965).

40. M. Dole, C. D. Keeling and D. G. Rose, "The Pile Irradiation of Polyethylene," J. Am. Chem. Soc. 76, 4304-11 (1954).

41. "Calibration Directions for F1100 Flowmeter," RGI, Inc., Vineland, New Jersey.

42. K. A. Browlee, Statistical Theory and Methodology in Science and Engineering, John Wiley & Sons, Inc., New York, 335-37 (1965).

43. "Least Squares Polynomial Regression Analysis Computer Program," Nuclear Engineering Department Computer Library, Kansas State University.

44. C. O. Bennett and J. E. Myers, Momentum, Heat and Mass Transfer, McGraw-Hill Book Company, Inc., New York, 385 (1962).

45. C. F. Bonilla, Nuclear Engineering, McGraw-Hill Book Company, Inc., New York, 397 (1957).

46. W. H. McAdams, Heat Transmission, McGraw-Hill Book Company, Inc., New York, 35-36 (1954).

47. A. B. Newman, "Heating and Cooling Rectangular and Cylindrical Solids," Ind. Eng. Chem. 28, 545-8 (1936).

11.0 APPENDICES

APPENDIX A

The Drying of Zinc and Manganous Carbonate Powders

The removal of adsorbed water from zinc and manganous carbonate powders required special consideration since they thermally decomposed below normal drying temperatures, approximately 100° C.

In this research a dry air system was used. The carbonates were vibration packed into stainless steel boats and placed into a glass tube. Dry air was then blown over them to pick up any adsorbed moisture. The dry air was generated by passing compressed air through a charcoal trap, then a drierite trap, and finally a liquid nitrogen trap. The effectiveness of these traps was shown by a color change, a moisture indication, in the drierite and the collection of water in the liquid nitrogen trap.

Weight losses of less than 1% of their original weight were observed after an 8 hour drying period for both carbonates. These losses showed no appreciable increases for longer drying periods.

APPENDIX B

The Calibration of the 90P3 Gas Chromatograph

The 90P3 gas chromatograph was absolutely calibrated for the quantitative analysis of carbon dioxide in a helium carrier gas. The calibration required that the integrated output for carbon dioxide from the thermal conductivity detector of the chromatograph be graphically or analytically related to known concentrations of carbon dioxide in helium-carbon dioxide mixtures.

With the chromatograph operating at the experimental conditions noted in the text, the response of the thermal conductivity detector plotted on the 1 mV scale of the strip chart recorder was in the form of Gaussian-shaped peaks for carbon dioxide. The method of determining the area under these peaks was by cutting the peak from the strip chart recorder paper and weighing. For constant peak areas, this technique was found to give a nominal standard deviation of 3% from the average of the peak weights.

Known concentrations of helium and carbon dioxide were obtained by flowing the two gases through tubing into each other at preset flow rates. The sources of the gases were commercial compressed gas cylinders fitted with suitable regulators. The mixture then was passed through the injection system of the chromatograph where samples of the mixture were analyzed.

The flow rates of helium and carbon dioxide were measured separately with the same RGI-F1100 flowmeter. The flowmeter was calibrated for the volumetric flow rate of both carbon dioxide and helium at 1 atmosphere pressure and 70° F in units of ml/min using the design instructions of the manufacturer (41). The calibration curves for the flowmeter are presented in Fig. 1B.

From the volumetric rate of flow of the two gases, the mole percentage of carbon dioxide in the mixture was obtained. Table I-B presents the peak

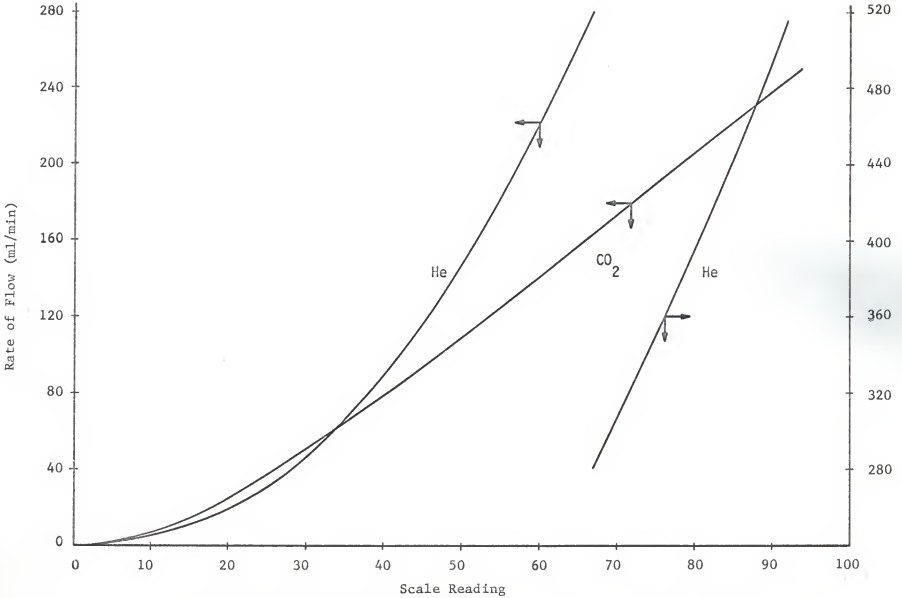

Fig. 1B. Helium and carbon dioxide calibration curves for RGI-F1100 flowmeter.

weights for carbon dioxide that were obtained for mole percentages of carbon dioxide in various gas mixtures.

Table I-B. Data for the Calibration of the 90P3 Chromatograph for Carbon Dioxide.

CO_2 Content of CO_2-Helium Mixture (mole percent)	Peak Weight (mg)
0.11	65.8
0.17	75.3
0.23	114.4
0.27	131.5
0.63	170.6
0.96	228.6
1.23	288.0
2.05	406.0
2.60	468.8
4.46	773.6
5.94	828.0
7.51	958.9
12.53	1760.0
17.52	1950.4
21.81	2676.5
22.71	2727.5
28.19	3291.2
31.36	3769.6
33.61	4153.6
52.38	6018.6
74.36	8864.0
100.00	12486.4

For graphical presentation the calibration was divided into three sections. In Fig. 2B the data from the origin up to 0.25 mole % CO_2 was fitted using linear least squares (42). Figs. 3B and 4B, which included the ranges 0.25-22.50 and 22.50-100 mole % CO_2, respectively, were both fitted by a regression analysis computer program (43) to less than 1% relative deviation with cubic polynomials. From these graphs, it was ascertained that a 3% standard deviation in the measurement of the peak weights would cause a nominal

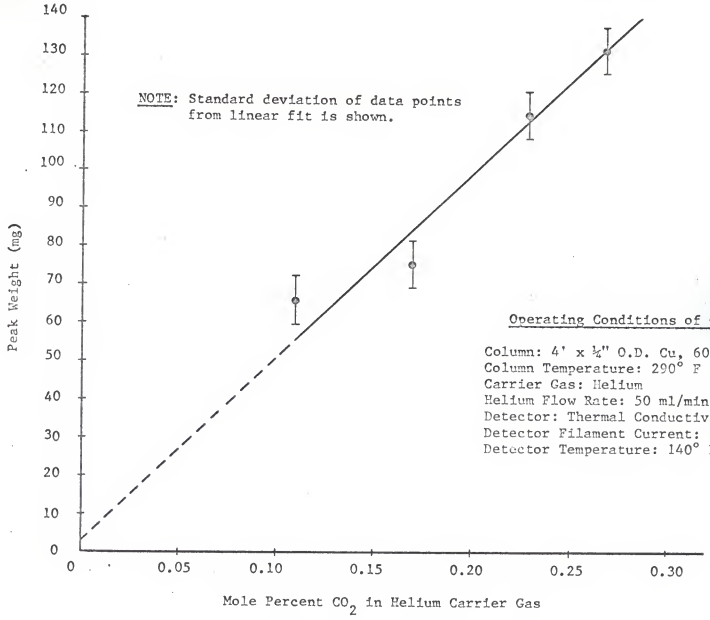

Fig. 2B. Calibration curve for helium mixtures with 0-0.25 mole percent CO_2 for 90P3 gas chromatograph.

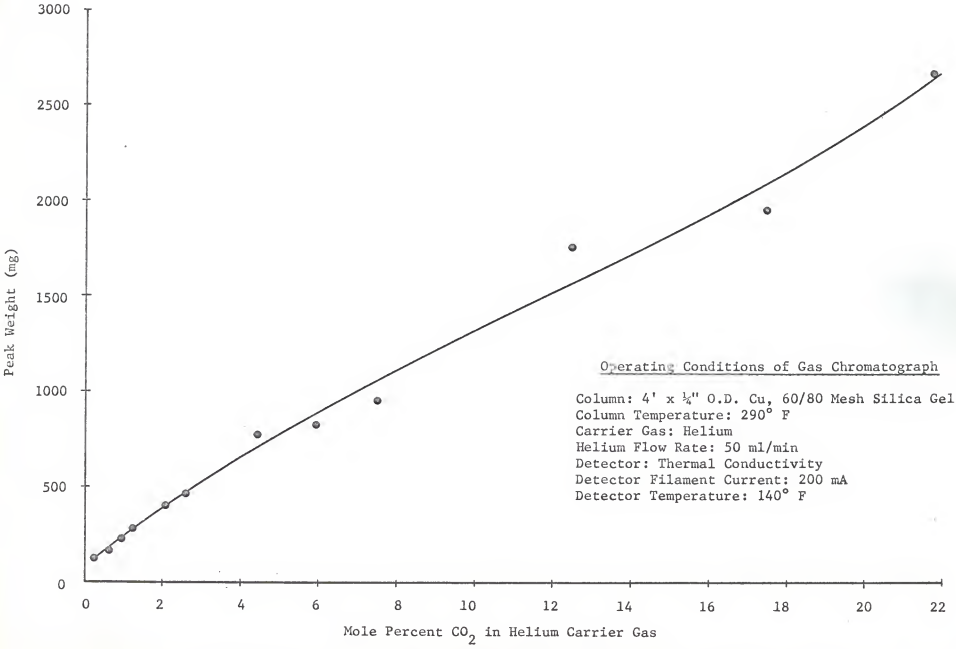

Fig. 3B. Calibration curve for helium mixtures with 0.25-22.50 mole percent CO_2 for 90P3 gas chromatograph.

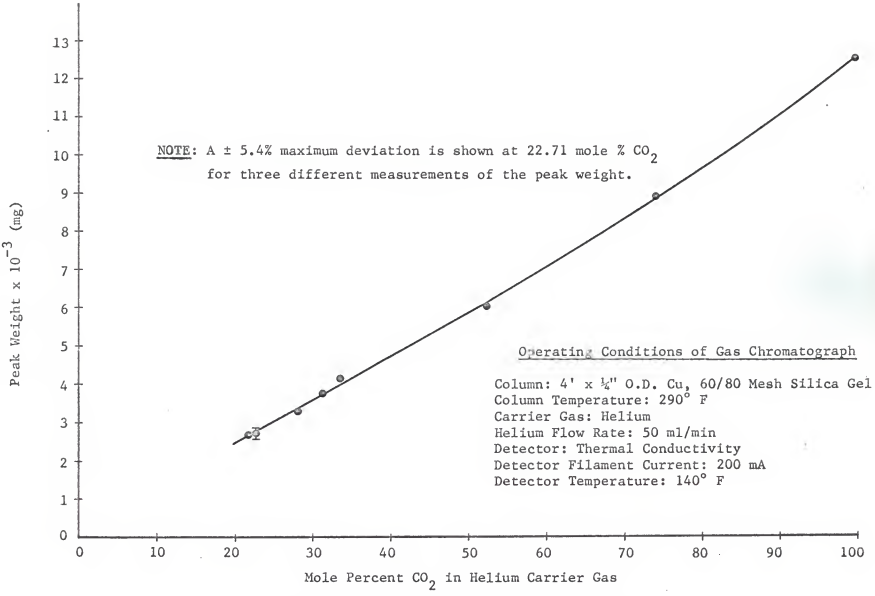

Fig. 4B. Calibration curve for helium mixtures with 22.50-100.00 mole percent CO_2 for 90P3 gas chromatograph.

error of 5% in the determination of the mole percentage of carbon dioxide.

APPENDIX C

A Correction for Thermocouple Radiation

The temperature within the flowing gas stream of a heated vessel may differ from the reading of a thermocouple placed in the gas stream. For such a case, a heat balance for the thermocouple

$$q_{gr} + q_c = q_r + q_k \tag{1C}$$

is used to compute the true gas temperature. q_{gr} is the rate of heat flow between gas and thermocouple by gas radiation, q_c is the rate of heat flow between gas and thermocouple by convection, q_r is the rate of radiant heat interchange between the thermocouple and the confining walls, and q_k is the rate of heat conduction from the thermocouple to the confining walls.

For a weak radiating gas such as helium and a well insulated thermocouple, q_{gr} and q_k are negligible when compared with q_c and q_r, and only thermocouple radiation must be considered. The general definition of the rate of heat flow, q, is

$$q = hA\Delta T \tag{2C}$$

where h is the heat transfer coefficient, A is the area of the surface normal to the heat flow, and ΔT is the temperature potential across which the heat is transferred. Eq. (1C) can then be written as

$$h_c A_t (T_g - T_t) = h_r A_t (T_t - T_w) \tag{3C}$$

where h_c is the convective heat transfer coefficient from the gas to the thermocouple, h_r is the radiative heat transfer coefficient from the thermocouple to the containment walls, and the subscripts t, g, and w denote the gas,

thermocouple, and confining wall, respectively.

Upon rearranging, Eq. (3C) is transformed to the form

$$T_g = T_t + \frac{h_r}{h_c}(T_t - T_w) \tag{4C}$$

which is used for finding the true gas temperature. From Eq. (4C), it is evident that the difference between the thermocouple reading and the true gas temperature increases with an increase in the temperature difference between the thermocouple and the walls, with an increase in the radiation coefficient, h_r, and with a decrease in the convection coefficient, h_c. Since h_r increases with temperature level much faster than h_c, the error in measuring the gas temperature will increase with temperature.

For the purposes of this research, the radiant heat transfer coefficient, h_r, was obtained with the relation (44)

$$h_r = \varepsilon_{t-w}\sigma \frac{(T_t^4 - T_w^4)}{T_t - T_w} \tag{5C}$$

where ε_{t-w} is the emissivity from the thermocouple to the walls, σ is the Stefan-Boltzman constant, and T_t and T_w are the absolute temperatures of the thermocouple and the wall. The convective heat transfer coefficient, h_c, was obtained from Bonilla's equation for flow past a single sphere (45)

$$\frac{h_c D}{k_g} = 0.80(D\bar{u}\rho_g/\mu)^{0.5}(C\mu/k_g)^{0.31} \tag{6C}$$

where k_g = thermal conductivity of gas, cal/sec·cm^2·(deg/cm)

$\bar{u}$ = average velocity of gas, cm/sec

μ = gas velocity, g/cm·sec

ρ_g = gas density, g/cm^3

D = sphere diameter or diameter of thermocouple tip, centimeters

C = specific heat of gas at constant pressure, cal/g·deg

APPENDIX D

Transient Heat Conduction in Carbonates

The Gurney-Lurie charts given in McAdams (46) were used in estimating the time required for a carbonate sample to reach equilibrium temperature in the high temperature furnace over the range 400-700° F. These charts presented graphical solutions to the transient heat conduction equation for a solid

$$\frac{k_s}{C_p} \nabla^2 T = \frac{\partial T}{\partial \Theta} \tag{1D}$$

for a number of simplified geometries.

The dimensionless groups used in the charts include:

1. a temperature change, Y

$$Y = \frac{T_a - T}{T_a - T_b} \tag{2D}$$

where T_a = temperature of surroundings, °F

T_b = original uniform temperature of solid, °F

T = temperature at position n at time Θ, °F

2. a relative time, x

$$x = \frac{k_s \Theta}{C_p r_m^2} \tag{3D}$$

where k_s = thermal conductivity of solid, Btu/h·ft^2·(deg/ft)

ρ = density of solid, lb/ft^3

C_p = specific heat of solid, Btu/lb·deg

Θ = time, from start of heating, hours

r_m = normal distance from midplane to surface, feet

3. a resistance ratio, m

$$m = \frac{k_s}{r_m h'} \tag{4D}$$

which h' = heat transfer coefficient between surroundings at T_a and surface at T_s, Btu/h·ft^2·deg

4. radius ratio, n

$$n = \frac{r'}{r_m} \tag{5D}$$

where r' = radius, normal distance from midplane to point in solid, feet.

So that the charts could be applied to the carbonate samples, they were assumed to be brick-shaped. They were further assumed to be insulated on the bottom side to account for the stainless steel boat touching the stainless steel heating tube.

For the brick-shaped carbonate insulated on one side, the thickness r_m in Eqs. (3D-5D) is replaced by the three dimensional values x_m, y_m, and z_m where z_m is the total thickness from the insulated bottom to the top of the carbonate. The value of Y at the midpoint of the carbonate was evaluated as a function of time by the method of Newmann (47) in which Y equals the product $Y_x Y_y Y_z$. Y_x, Y_y, and Y_z are evaluated individually from the Gurney-Lurie charts for a large slab. The midpoint temperature as a function of time was calculated from these values of Y. The time for the carbonate to reach equilibrium was found by observing the midpoint temperature of the carbonate with time. The results of these calculations are presented in Fig. 1D.

The constants used for these calculations were:

k_s = 0.35 Btu/h·ft^2·(deg/ft)

ρ = 49.7 lb/ft^3

C_p = 0.25 Btu/lb·deg

x_m = 0.01172 ft

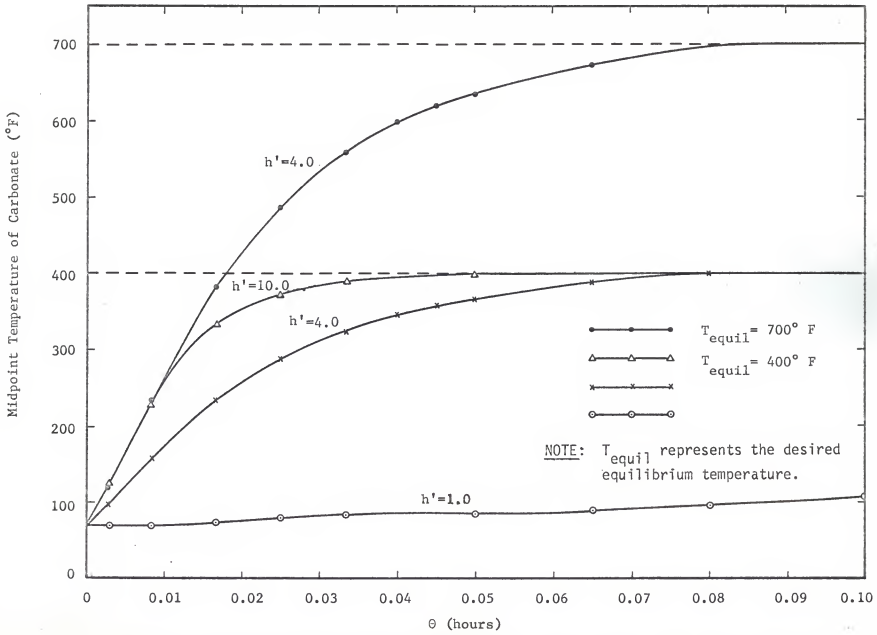

Fig. 1D. The time required for carbonate samples to reach thermal equilibrium at 400° F and 700° F following a step change from room temperature.

y_m = 0.05339 ft

z_m = 0.01823 ft

h' = 1-10 Btu/h·ft^2·deg

k_s, ρ, and C_p were estimated from values given in McAdams (46) for materials similar to the carbonates and were assumed to be fairly constant with temperature. Since h' could not be directly calculated either, an overall range was estimated.

APPENDIX E

Data for the Thermal Decomposition of the Powdered Carbonates

Table I-E. CO_2 Production Rate with Time for Unirradiated $ZnCO_3$ at 189° C.

Time (min)	CO_2 Production Rate (ml/min·g dried carbonate) Run No. 1	Run No. 2	Run No. 3	Run No. 4	Average
2	0.0151	0.0235	0.0146	0.0096	0.0157±0.0058
4	0.1517	0.1817	0.1573	0.1545	0.1613±0.0138
6	0.0653	0.0945	0.0767	0.0775	0.0785±0.0120
8	0.0306	0.0459	0.0150	0.0383	0.0325±0.0132
10	0.0162	0.0249	0.0239	0.0195	0.0211±0.0040
12	0.0104	0.0145	0.0125	0.0117	0.0123±0.0017
14	0.0086	0.0111	0.0103	0.0094	0.0098±0.0008
16	0.0080	0.0092	0.0093	0.0087	0.0088±0.0006
18	0.0071	0.0091	0.0091	0.0083	0.0084±0.0009
20	0.0069	0.0090	0.0087	0.0078	0.0081±0.0009
22	0.0070	0.0085	0.0085	0.0083	0.0081±0.0007
24	0.0069	0.0092	0.0091	0.0083	0.0084±0.0011
26	0.0068	0.0092	0.0091	0.0085	0.0084±0.0011
28	0.0073	0.0094	0.0095	0.0088	0.0088±0.0010
30	0.0073	0.0099	0.0103	0.0089	0.0091±0.0013
32	0.0073	0.0091	0.0100	0.0090	0.0089±0.0011
34	0.0078	0.0102	0.0100	0.0092	0.0093±0.0011
36	0.0075	0.0102	0.0103	0.0091	0.0093±0.0013
38	0.0075	0.0101	0.0101	0.0093	0.0092±0.0012
40	0.0079	0.0101	0.0102	0.0096	0.0095±0.0011
42	0.0077	0.0103	0.0103	0.0092	0.0094±0.0012
44	0.0075	0.0100	0.0103	0.0095	0.0093±0.0013
46	0.0078	0.0099	0.0104	0.0095	0.0094±0.0011
48	0.0077	0.0103	0.0104	0.0094	0.0095±0.0012
50	0.0076	0.0104	0.0103	0.0093	0.0094±0.0013
52	0.0076	0.0099	0.0101	0.0096	0.0093±0.0011
54	0.0075	0.0104	0.0105	0.0094	0.0095±0.0014
56	0.0076	0.0102	0.0100	0.0093	0.0093±0.0012
58	0.0078	0.0100	0.0100	0.0093	0.0093±0.0010
60	0.0079	0.0104	0.0103	0.0090	0.0094±0.0012
Total CO_2 (ml/g dried sample)	0.9398	1.2422	1.0950	1.0556	1.0832±0.1248
W_s (g)	0.9981	0.9584	1.0012	0.9659	
W_1 (g)	0.0337	0.0331	0.0366	0.0353	

Table II-E. CO_2 Production Rate with Time for Irradiated $ZnCO_3$ at 189° C.

Time (min)	CO_2 Production Rate (ml/min·g dried carbonate) 9.45 Mrad Run No. 1	Run No. 2	Run No. 3	Average	18.8 Mrad
2	0.0539	0.0864	0.0880	0.0761±0.0192	0.0800
4	0.1921	0.1776	0.1786	0.1828±0.0081	0.2149
6	0.0800	0.0685	0.0661	0.0715±0.0074	0.0794
8	0.0410	0.0351	0.0327	0.0363±0.0043	0.0422
10	0.0245	0.0231	0.0176	0.0217±0.0036	0.0315
12	0.0154	0.0147	0.0123	0.0141±0.0016	0.0261
14	0.0129	0.0114	0.0112	0.0118±0.0009	0.0329
16	0.0127	0.0117	0.0103	0.0116±0.0012	0.0329
18	0.0124	0.0120	0.0106	0.0117±0.0009	0.0315
20	0.0124	0.0118	0.0102	0.0115±0.0011	0.0320
22	0.0129	0.0130	0.0100	0.0120±0.0017	0.0301
24	0.0127	0.0132	0.0107	0.0122±0.0015	0.0249
26	0.0124	0.0121	0.0106	0.0117±0.0010	0.0234
28	0.0125	0.0126	0.0099	0.0117±0.0015	0.0209
30	0.0124	0.0123	0.0106	0.0118±0.0010	0.0160
32	0.0124	0.0125	0.0099	0.0116±0.0013	0.0163
34	0.0119	0.0132	0.0093	0.0115±0.0020	0.0146
36	0.0118	0.0116	0.0102	0.0112±0.0009	0.0122
38	0.0114	0.0111	0.0099	0.0108±0.0008	0.0123
40	0.0113	0.0113	0.0088	0.0105±0.0014	0.0120
42	0.0119	0.0111	0.0096	0.0109±0.0012	0.0110
44	0.0115	0.0110	0.0092	0.0106±0.0012	0.0114
46	0.0111	0.0110	0.0083	0.0101±0.0016	0.0112
48	0.0113	0.0110	0.0085	0.0103±0.0015	0.0106
50	0.0111	0.0107	0.0084	0.0102±0.0015	0.0112
52	0.0110	0.0107	0.0079	0.0099±0.0017	0.0104
54	0.0110	0.0104	0.0080	0.0098±0.0016	0.0102
56	0.0110	0.0103	0.0079	0.0097±0.0016	0.0099
58	0.0108	0.0103	0.0077	0.0096±0.0017	0.0104
60	0.0107	0.0099	0.0076	0.0094±0.0016	0.0094
Total CO_2 (ml/g dried sample)	1.3808	1.3632	1.2412	1.3284±0.0760	1.7836
W_s (g)	0.9632	1.1015	1.0182		0.9982
W_1 (g)	0.0404	0.0463	0.0392		0.0451

Table III-E. CO_2 Production Rate with Time for Unirradiated and Irradiated $ZnCO_3$ at 242° C and 292° C.

Time (min)	CO_2 Production Rate (ml/min·g dried carbonate) 242° C Unirradiated	242° C 9.45 Mrad	292° C Unirradiated	292° C 9.45 Mrad
2	0.2118	0.2839	3.8544	5.3173
4	0.2750	0.2936	9.4883	9.8691
6	0.6051	0.6331	8.0654	8.1163
8	1.0701	1.0113	4.9883	3.5392
10	2.3605	2.1550	2.2622	1.9580
12	2.9717	2.8454	1.1642	0.8027
14	3.0699	2.9985	0.3888	0.3543
16	3.1796	2.9985	0.2301	0.2290
18	2.8865	2.5110	0.1541	0.1531
20	2.4007	2.2342	0.1137	0.1183
22	2.0808	1.8892	0.0885	0.0923
24	1.8437	1.8042	0.0735	0.0722
26	1.4239	1.5110	0.0606	0.0633
28	1.1173	1.2902	0.0473	0.0516
30	0.8882	1.0297	0.0430	0.0429
32	0.5440	0.7207	0.0359	0.0358
34	0.3553	0.4237	0.0326	0.0273
36	0.2308	0.2836	0.0269	0.0251
38	0.1337	0.1602	0.0209	0.0202
40	0.0776	0.1040	0.0180	0.0153
42	0.0462	0.0616	0.0164	0.0149
44	0.0218	0.0336	0.0132	0.0129
46	0.0129	0.0168	0.0125	0.0124
48	0.0098	0.0117	0.0119	0.0113
50	0.0080	0.0087	0.0112	0.0106
52	0.0070	0.0079	0.0104	0.0098
54	0.0065	0.0066	0.0100	0.0091
56	0.0053	0.0060	0.0091	0.0082
58	0.0051	0.0054	0.0087	0.0076
60	0.0048	0.0051	0.0081	0.0067
Total CO_2 (ml/g dried sample)	27.8536	27.3444	62.5364	62.0136
W_s (g)	1.0379	1.0305	1.0901	0.9678
W_1 (g)	0.2437	0.2470	0.2794	0.2478

Table IV-E. CO_2 Production Rate with Time for Unirradiated and Irradiated $MnCO_3$ at 242° C and 345° C.

Time (min)	CO_2 Production Rate (ml/min·g dried carbonate) 242° C Unirradiated	242° C 9.45 Mrad	345° C Unirradiated	345° C 9.45 Mrad
2	0.0124	0.0217	0.4877	0.5049
4	0.0426	0.0551	0.9222	1.0434
6	0.0148	0.0199	0.4760	0.5302
8	0.0066	0.0081	0.3477	0.2907
10	0.0050	0.0062	0.3967	0.3403
12	0.0041	0.0051	0.4648	0.4764
14	0.0050	0.0044	0.5192	0.5613
16	0.0043	0.0046	0.5063	0.5480
18	0.0041	0.0041	0.5419	0.5696
20	0.0040	0.0041	0.5208	0.5530
22	0.0037	0.0040	0.5192	0.5745
24	0.0035	0.0033	0.5321	0.5563
26	0.0033	0.0036	0.5468	0.5712
28	0.0032	0.0034	0.5614	0.5895
30	0.0031	0.0033	0.5484	0.6045
32	0.0031	0.0033	0.5565	0.5862
34	0.0030	0.0031	0.5419	0.6045
36	0.0029	0.0031	0.5745	0.5912
38	0.0031	0.0031	0.5630	0.5961
40	0.0028	0.0031	0.5565	0.5995
42	0.0029	0.0031	0.5582	0.6095
44	0.0029	0.0031	0.5630	0.6361
46	0.0029	0.0030	0.5876	0.6161
48	0.0029	0.0031	0.5435	0.6211
50	0.0029	0.0029	0.5810	0.6078
52	0.0029	0.0030	0.5614	0.6244
54	0.0030	0.0031	0.5925	0.5978
56	0.0029	0.0030	0.5663	0.6427
58	0.0029	0.0031	0.5663	0.6161
60	0.0030	0.0030	0.5745	0.6228
Total CO_2 (ml/g dried sample)	0.3276	0.3940	32.7558	34.9714
W_s (g)	1.5283	1.5184	1.3644	1.3410
W_1 (g)	0.0162	0.0200	0.2588	0.2637

Table V-E. CO_2 Production Rate with Time for Unirradiated $MnCO_3$ at 292° C.

Time (min)	CO_2 Production Rate (ml/min·g dried carbonate) Run No. 1	Run No. 2	Run No. 3	Average	18.8 Mrad Control
2	0.0504	0.0130	0.0374	0.0336±0.0190	0.0007
4	0.1560	0.1025	0.1529	0.1371±0.0300	0.1389
6	0.1813	0.1876	0.1897	0.1862±0.0044	0.1977
8	0.2780	0.2967	0.2611	0.2786±0.0178	0.2911
10	0.3279	0.3321	0.3384	0.3328±0.0053	0.3168
12	0.2387	0.2122	0.2537	0.2349±0.0210	0.2447
14	0.1285	0.1406	0.1414	0.1368±0.0072	0.1480
16	0.0769	0.0845	0.0877	0.0830±0.0055	0.0938
18	0.0485	0.0536	0.0503	0.0508±0.0026	0.0595
20	0.0289	0.0346	0.0334	0.0323±0.0030	0.0400
22	0.0222	0.0227	0.0246	0.0232±0.0013	0.0279
24	0.0163	0.0191	0.0184	0.0179±0.0015	0.0191
26	0.0144	0.0143	0.0169	0.0152±0.0015	0.0158
28	0.0133	0.0142	0.0145	0.0140±0.0006	0.0131
30	0.0123	0.0139	0.0133	0.0132±0.0008	0.0123
32	0.0128	0.0131	0.0151	0.0137±0.0012	0.0111
34	0.0115	0.0111	0.0118	0.0115±0.0004	0.0111
36	0.0116	0.0113	0.0133	0.0121±0.0011	0.0110
38	0.0116	0.0112	0.0132	0.0120±0.0011	0.0104
40	0.0104	0.0105	0.0131	0.0113±0.0015	0.0102
42	0.0113	0.0112	0.0130	0.0118±0.0010	0.0096
44	0.0104	0.0108	0.0132	0.0115±0.0015	0.0098
46	0.0123	0.0105	0.0134	0.0121±0.0015	0.0098
48	0.0104	0.0100	0.0122	0.0109±0.0012	0.0092
50	0.0110	0.0105	0.0121	0.0112±0.0008	0.0096
52	0.0109	0.0103	0.0123	0.0112±0.0010	0.0095
54	0.0110	0.0100	0.0115	0.0108±0.0008	0.0103
56	0.0107	0.0107	0.0123	0.0112±0.0009	0.0097
58	0.0119	0.0104	0.0112	0.0112±0.0008	0.0105
60	0.0106	0.0116	0.0118	0.0113±0.0006	0.0098
Total CO_2 (ml/g dried sample)	3.5240	3.4096	3.6464	3.5267±0.1184	3.5420
W_s (g)	1.3624	1.2549	1.2688		1.3564
W_1 (g)	0.0508	0.0441	0.0475		0.0473

Table VI-E. CO_2 Production Rate with Time for Irradiated $MnCO_3$ at 292° C.

Time (min)	CO_2 Production Rate (ml/min·g dried carbonate) 9.45 Mrad Run No. 1	Run No. 2	Run No. 3	Average	18.8 Mrad
2	0.0659	0.0699	0.0500	0.0619 0.0105	0.0075
4	0.1242	0.1482	0.1857	0.1527 0.0310	0.1470
6	0.1480	0.1835	0.2319	0.1878 0.0421	0.2441
8	0.2324	0.3037	0.3551	0.2971 0.0616	0.3556
10	0.3194	0.2196	0.3544	0.2978 0.0699	0.3065
12	0.2545	0.2291	0.2367	0.2401 0.0130	0.2126
14	0.1401	0.1262	0.1295	0.1319 0.0073	0.1260
16	0.0817	0.0706	0.0755	0.0759 0.0056	0.0758
18	0.0515	0.0427	0.0469	0.0470 0.0044	0.0449
20	0.0318	0.0309	0.0309	0.0312 0.0005	0.0326
22	0.0236	0.0216	0.0248	0.0233 0.0016	0.0224
24	0.0162	0.0176	0.0209	0.0182 0.0024	0.0187
26	0.0155	0.0155	0.0202	0.0171 0.0027	0.0186
28	0.0149	0.0143	0.0173	0.0155 0.0016	0.0177
30	0.0145	0.0141	0.0171	0.0152 0.0016	0.0171
32	0.0132	0.0141	0.0173	0.0149 0.0022	0.0163
34	0.0117	0.0122	0.0178	0.0139 0.0034	0.0163
36	0.0121	0.0134	0.0185	0.0147 0.0034	0.0161
38	0.0134	0.0120	0.0181	0.0145 0.0032	0.0166
40	0.0126	0.0136	0.0179	0.0147 0.0028	0.0169
42	0.0137	0.0116	0.0170	0.0141 0.0027	0.0157
44	0.0114	0.0143	0.0185	0.0147 0.0036	0.0155
46	0.0127	0.0117	0.0184	0.0143 0.0036	0.0155
48	0.0121	0.0122	0.0174	0.0139 0.0030	0.0180
50	0.0123	0.0129	0.0182	0.0145 0.0032	0.0168
52	0.0120	0.0116	0.0174	0.0137 0.0032	0.0173
54	0.0115	0.0133	0.0174	0.0141 0.0029	0.0163
56	0.0119	0.0120	0.0170	0.0136 0.0029	0.0164
58	0.0113	0.0118	0.0167	0.0133 0.0039	0.0157
60	0.0115	0.0121	0.0167	0.0134 0.0028	0.0155
Total CO_2 (ml/g dried sample)	3.4352	3.3926	4.1221	3.6500 0.4094	3.7840
W_s (g)	1.3643	1.4049	1.3742		1.4329
W_1 (g)	0.0503	0.0508	0.0542		0.0523

Table VII-E. CO_2 Production Rate with Time for Unirradiated $MnCO_3$ at 396° C.

Time (min)	CO_2 Production Rate (ml/min·g dried sample) Helium Flow = 4 ml/min	Helium Flow = 1.3 ml/min
2	1.2973	0.2584
4	1.9397	0.9537
6	4.5362	2.1261
8	7.4270	3.5709
10	8.0249	5.5055
12	9.4556	5.5593
14	9.4511	6.0089
16	7.5209	6.1400
18	7.6720	6.0089
20	6.2325	5.9713
22	5.8419	5.5235
24	5.1469	4.8941
26	4.4775	4.7738
28	3.4767	4.0213
30	2.5409	3.9130
32	1.5719	3.0695
34	0.7682	2.7984
36	0.2026	2.2838
38	0.0606	1.6231
40	0.0165	0.1118
42	0.0090	0.5770
44	0.0062	0.4558
46	0.0047	0.3198
48	0.0041	0.2274
50	0.0033	0.1531
52	0.0029	0.1012
54	0.0024	0.0632
56	0.0021	0.0392
58	0.0018	0.0260
60	0.0018	0.0178
Total CO_2 (ml/g dried sample)	175.4336	156.2896
W_s (g)	1.2037	1.2173
W_1 (g)	0.4482	0.4597

THE EFFECTS OF CO-60 GAMMA RADIATION ON THE THERMAL DECOMPOSITION OF CARBONATE COMPOUNDS

by

DANNY WILLIAM LABELLE

B. S., North Carolina State University, 1966

AN ABSTRACT OF A MASTER'S THESIS

submitted in partial fulfillment of the

requirements for the degree

MASTER OF SCIENCE

Department of Nuclear Engineering

KANSAS STATE UNIVERSITY

Manhattan, Kansas

1969

ABSTRACT

Powdered zinc and manganous carbonates were isothermally decomposed to metallic oxides and carbon dioxide gas in an inert atmosphere of flowing helium at various temperatures between 180 and 400° C. The decompositions were studied by periodically measuring the carbon dioxide content of the helium flow with a gas chromatography system. These measurements were used to calculate the carbon dioxide production rate with time for each of the decompositions. The carbonates were also isothermally decomposed at similar temperatures after receiving cobalt-60 gamma irradiations. Definite effects of the pre-irradiation treatment on the decompositions were ascertained by comparison of the carbon dioxide production rates obtained with and without irradiation. Plots and tables of all the time-dependent carbon dioxide production rates are included.

The helium flow rate across the carbonates was shown to influence the rate of decomposition. It was further shown that the method of sample preparation, particle size, and impurity content of the carbonates may also influence the rate of decomposition.

The decomposition of the powdered zinc carbonate was determined to be governed by first order kinetics during the early stages of its decomposition, eventually becoming diffusion-limited. The manganous carbonate was determined to have a diffusion-controlled decomposition; the major portion of the decomposition was governed by the one-third power law for contracting spheres.